Transfer of ion binding site from ether-à-go-go to Shaker: Mg^{2+} binds to resting state to modulate channel opening

Meng-chin A. Lin,[1] Jeff Abramson,[1] and Diane M. Papazian[1,2,3]

[1]Department of Physiology, [2]Molecular Biology Institute, and [3]Brain Research Institute, David Geffen School of Medicine, University of California, Los Angeles, Los Angeles, CA 90095

In ether-à-go-go (eag) K^+ channels, extracellular divalent cations bind to the resting voltage sensor and thereby slow activation. Two eag-specific acidic residues in S2 and S3b coordinate the bound ion. Residues located at analogous positions are ~4 Å apart in the x-ray structure of a Kv1.2/Kv2.1 chimera crystallized in the absence of a membrane potential. It is unknown whether these residues remain in proximity in Kv1 channels at negative voltages when the voltage sensor domain is in its resting conformation. To address this issue, we mutated Shaker residues I287 and F324, which correspond to the binding site residues in eag, to aspartate and recorded ionic and gating currents in the presence and absence of extracellular Mg^{2+}. In I287D+F324D, Mg^{2+} significantly increased the delay before ionic current activation and slowed channel opening with no readily detectable effect on closing. Because the delay before Shaker opening reflects the initial phase of voltage-dependent activation, the results indicate that Mg^{2+} binds to the voltage sensor in the resting conformation. Supporting this conclusion, Mg^{2+} shifted the voltage dependence and slowed the kinetics of gating charge movement. Both the I287D and F324D mutations were required to modulate channel function. In contrast, E283, a highly conserved residue in S2, was not required for Mg^{2+} binding. Ion binding affected activation by shielding the negatively charged side chains of I287D and F324D. These results show that the engineered divalent cation binding site in Shaker strongly resembles the naturally occurring site in eag. Our data provide a novel, short-range structural constraint for the resting conformation of the Shaker voltage sensor and are valuable for evaluating existing models for the resting state and voltage-dependent conformational changes that occur during activation. Comparing our data to the chimera x-ray structure, we conclude that residues in S2 and S3b remain in proximity throughout voltage-dependent activation.

INTRODUCTION

High resolution x-ray structures have been reported for two mammalian voltage-gated K^+ channels, Kv1.2 and a Kv1.2/Kv2.1 chimera (Long et al., 2005a, 2007). These structures, obtained in the absence of a membrane potential, capture the channel protein in its lowest energy conformation, which presumably corresponds to an inactivated state. In contrast, no high resolution structural data are available for the higher-energy, resting conformation, which is adopted in the presence of a negative transmembrane voltage.

In the absence of crystallographic data, indirect structural constraints are of considerable value in modeling protein structure (Papazian et al., 1995; Tiwari-Woodruff et al., 1997, 2000; Silverman et al., 2000, 2003; Lainé et al., 2003). However, relatively few constraints for the resting conformation of voltage-gated ion channels have been reported (Tombola et al., 2005; Campos et al., 2007). To probe the structure of the resting state in Kv1 channels, we investigated whether a functional binding site for divalent cations could be transferred from ether-à-go-go (eag) to the Shaker voltage sensor domain.

In voltage-gated eag K^+ channels, the binding of extracellular Mg^{2+}, Ca^{2+}, or other divalent cations to a site in the voltage sensor domain significantly slows activation (Terlau et al., 1996; Tang et al., 2000; Silverman et al., 2003, 2004). Channel kinetics are maximally sensitive to changes in Mg^{2+} or Ca^{2+} in the physiological concentration range, with half-maximal effective concentrations in the low millimolar range (Silverman et al., 2000). Using a combination of gating current and optical measurements, we showed that Mg^{2+} primarily affects voltage-dependent transitions between deep closed states that occur at hyperpolarized voltages (Tang et al., 2000; Silverman et al., 2004; Bannister et al., 2005). These rate-limiting transitions are poorly represented in gating current records, but are readily detected by a fluorescent reporter attached to the extracellular loop between transmembrane segments S3 and S4 (Bannister et al., 2005). Mg^{2+}-modulated transitions have a more hyperpolarized voltage dependence than other steps in eag activation, indicating that Mg^{2+} is able to bind to the deepest closed (resting) conformation of the voltage

Correspondence to Diane M. Papazian: papazian@mednet.ucla.edu

Abbreviations used in this paper: eag, ether-à-go-go; τ_{act}, activation time constant; τ_{deact}, deactivation time constant; τ_{on}, ON gating current time constant.

The Rockefeller University Press $30.00
J. Gen. Physiol. Vol. 135 No. 5 415–431
www.jgp.org/cgi/doi/10.1085/jgp.200910320

sensor domain (Silverman et al., 2004; Bannister et al., 2005). Mg^{2+} slows activation by shifting the voltage dependence of rate-limiting transitions in the depolarized direction (Terlau et al., 1996; Bannister et al., 2005).

Two aspartate residues, one each in S2 and S3b in the eag voltage sensor domain, contribute to the binding site for extracellular divalent cations (Silverman et al., 2000) (Fig. 1). These positions, which correspond to D278 and D327 in *Drosophila* eag, are occupied by negatively charged residues only among members of the eag subfamily and the related CNG channel subfamily (Kaupp et al., 1989; Dhallan et al., 1990; Warmke et al., 1991; Warmke and Ganetzky, 1994; Nelson et al., 1999) (Fig. 1 A). We have shown that mutating either D278 or D327 to a neutral residue slows eag activation kinetics similarly to ion binding, indicating that charge shielding by the bound ion is important for reducing the rate of channel opening (Silverman et al., 2000). We have also shown that D278 and D327 project into an external gating crevice that contains the side chain of D274, the eag analogue of an acidic residue in S2 that is highly conserved in the superfamily of voltage-gated ion channels (Fig. 1). In eag, D274 is not required for ion binding, nor does it contribute to the apparent affinity for Mg^{2+} (Silverman et al., 2000). Instead, this widely conserved acidic residue interacts with charge-moving arginine residues in S4 during voltage-dependent activation (Tiwari-Woodruff et al., 1997, 2000; Silverman et al., 2003).

Before high resolution x-ray structures of mammalian Kv channels were available, we used the binding site in eag as a structural constraint, in combination with intragenic suppression results from Shaker and data from the literature, to model the Shaker channel in an open conformation (Lainé et al., 2003; Silverman et al., 2003). This model predicted several structural features later confirmed in the Kv1.2 and Kv1.2/Kv2.1 chimera x-ray structures, including the packing arrangement of transmembrane segments in the voltage sensor domain; the existence of two networks of charged interactions between specific residues in S2, S3, and S4; and the association of the voltage sensor domain from one subunit with the pore domain of the adjacent subunit in the clockwise direction, viewed from an extracellular perspective (Lainé et al., 2003; Silverman et al., 2003; Long et al., 2005a, 2007). In the chimera x-ray structure, the side chains of I230 in S2 and Y267 in S3b, which correspond to the binding site residues in eag, are ~4 Å apart at their closest point. Thus, the binding site in eag proved to be an excellent constraint for modeling Kv1 channel structure at 0 mV.

Whereas functional results obtained with eag provide strong evidence that the binding site residues are in proximity in the resting conformation, the analogous residues are closely apposed at 0 mV in the x-ray structure of the Kv1.2/Kv2.1 chimera (Tang et al., 2000; Silverman et al., 2004; Bannister et al., 2005; Long et al., 2007). Whether these residues remain in proximity in the resting state of Shaker-type channels is unknown. To address this question, we investigated whether a functional divalent cation binding site could be engineered in the Shaker voltage sensor domain. We mutated I287 and F324 in Shaker to aspartate residues and compared channel function in the presence and absence of external Mg^{2+} (Fig. 1). We report that acidic residues engineered into S2 and S3b of the Shaker voltage sensor domain generate a functional divalent cation binding site that strongly resembles the one in eag. The data indicate that the engineered binding site residues are closely apposed in both resting and activated voltage sensor conformations in Shaker. Our results strongly suggest that the binding site residues in S2 and S3b maintain their proximity during voltage-dependent activation. Therefore, the data argue against the idea that S3b and S4 move together as a voltage sensor paddle unit during activation (Jiang et al., 2003; Long et al., 2005b; Ruta et al., 2005; Alabi et al., 2007). Our findings provide a robust constraint for modeling the structure of the resting conformation and the conformational changes that occur during activation.

MATERIALS AND METHODS

Molecular biology

Mutations were made in the noninactivating Shaker-IR cDNA clone, which contains a deletion of residues 6–46 to remove N-type inactivation (Hoshi et al., 1990). For gating current experiments, the W434F mutation was introduced to eliminate ionic currents (Perozo et al., 1993). Mutations were generated using the QuikChange method (Agilent Technologies) or by PCR using a four-primer strategy (Landt et al., 1990). Mutations were verified by sequencing. DNA was linearized with EcoRI for in vitro transcription using the mMessage mMachine T7 or T7 Ultra kit (Applied Biosystems). RNA was injected into *Xenopus* oocytes using standard methods (Timpe et al., 1988; Papazian et al., 1991).

Ionic current experiments

1–2 d after RNA injection, ionic currents were recorded at room temperature (20–22°C) using a two-electrode voltage clamp (OC-725C; Warner Instruments) (Timpe et al., 1988; Papazian et al., 1991). Electrodes were filled with 3 M KCl and had resistances of 0.3–1.0 MΩ. Oocytes were bathed in 96 mM NaCl, 2 mM KCl, 0.5 mM $CaCl_2$, and 5 mM HEPES, pH 7.5. To record tail currents, 96 mM NaCl plus 2 mM KCl was replaced by 98 mM KCl. In some experiments, the 2-mM KCl bath solution was buffered to pH 8.0 with HEPES or to pH 5.5 or 6.5 with MES (2-(*N*-morpholino)ethanesulfonic acid). Extracellular 10 mM $MgCl_2$ was added as indicated.

Pulse protocols were generated and data were acquired using pClamp software and a TL-1 Labmaster interface (Axon Instruments). Data were sampled at 0.8–2 kHz and filtered at one fifth the sampling frequency using an eight-pole Bessel filter (Frequency Devices). The sampling rate was varied as needed to characterize activation and deactivation kinetics. Linear capacitive and leak currents were subtracted using a P/−4 protocol (Bezanilla and Armstrong, 1977).

Currents were evoked by pulsing from a holding potential of −100 mV to voltages ranging from −60 to +90 mV in 10-mV

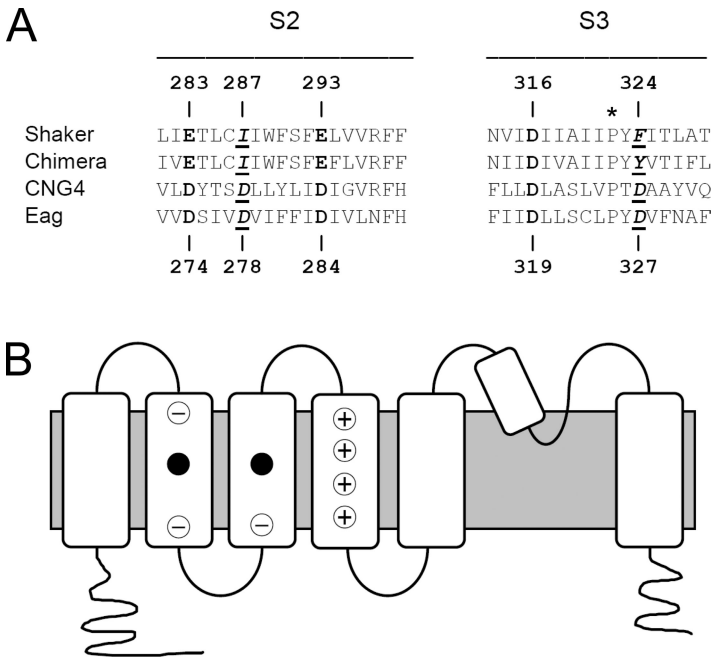

Figure 1. Alignment of S2 and S3 sequences from Shaker, the Kv1.2/Kv2.1 chimera, Drosophila eag, and rat CNG4 (A) (Tempel et al., 1987; Warmke et al., 1991; Chandy and Gutman, 1995; Nelson et al., 1999; Long et al., 2007). Acidic residues conserved throughout the voltage-gated channel superfamily are shown in bold; positions of acidic residues conserved only in the eag and CNG subfamilies are underlined and shown in bold italics. The asterisk (*) above the conserved proline in S3 indicates the division between S3a and S3b (Alabi et al., 2007). Numbers corresponding to the Shaker and eag sequences are provided above and below the alignment, respectively. (B) Cartoon of the membrane topology of a voltage-gated K^+ channel subunit shows the approximate locations of the binding site residues (filled circles) (Silverman et al., 2000). Circled negative signs indicate positions occupied by acidic residues throughout the voltage-gated channel superfamily (Chandy and Gutman, 1995). Circled positive signs indicate charge-moving arginine residues in the S4 segment (Aggarwal and MacKinnon, 1996; Seoh et al., 1996). Filled circles indicate positions occupied by acidic residues only in the eag and CNG channel subfamilies (Kaupp et al., 1989; Dhallan et al., 1990; Warmke and Ganetzky, 1994).

increments. Current traces were fitted with single- or double-exponential functions, as needed, to obtain activation time constant (τ_{act}) values. To estimate the delay before the detection of ionic currents, the fitted exponential functions were extrapolated to 0 current amplitude; the delay was measured as the difference between this intercept and the start of the voltage pulse ($t = 0$) (Perozo et al., 1994). Deactivation kinetics were characterized by recording tail currents in the 98-mM KCl bath solution. The membrane was stepped to +40 mV before repolarizing to a series of tail potentials. Tail currents were fitted with a single-exponential function to determine deactivation time constant (τ_{deact}) values. Values of τ_{act} and τ_{deact} are provided as mean ± SEM. Statistical significance was assessed using a one-way ANOVA.

In the control channel (Shaker-IR) and the I287D and F324D single-mutant channels, ionic conductance saturated within the tested voltage range. For these constructs, the normalized conductance (g/g_{max}) was determined as a function of voltage. The conductance was calculated using the equation $g = I/(V\text{-}V_{rev})$, where I is the steady-state current amplitude at voltage V. V_{rev} was assumed to be −95 mV, calculated using the Nernst equation. Conductance values were normalized using the maximum value obtained in the experiment. g-V data were fitted with a single Boltzmann function using Origin 7.0 (Microcal), providing values for the midpoint potential ($V_{1/2}$) and apparent valence. In the I287D+F324D and E283A+I287D+F324D channels, conductance did not saturate within the tested voltage range. To characterize their steady-state activation properties, conductance values from individual experiments were plotted without normalization versus voltage. To obtain values for $V_{1/2}$ and the apparent valence, data were fitted with a single Boltzmann function without constraining the upper value of the conductance. Fitted parameters from individual experiments were averaged and are reported as mean ± SEM.

The addition of 10 mM Mg^{2+} to the bath solution resulted in a surface charge effect that shifted the g-V curve in the depolarized direction (Elinder and Århem, 2003; Broomand et al., 2007; Lin and Papazian, 2007). The Ca^{2+} concentration in the bath solution was purposely kept low (0.5 mM) because Ca^{2+}, like Mg^{2+}, binds to the divalent cation site in eag (Lin and Papazian, 2007). This concentration of Ca^{2+} was insufficient to offset the surface charge effect of 10 mM Mg^{2+} (Lin and Papazian, 2007). Values of τ_{act} and τ_{deact} obtained in the presence of extracellular Mg^{2+} were plotted versus the applied voltage and versus the voltage obtained after correcting for the surface charge effect.

Gating current experiments

Gating currents were recorded using a cut-open oocyte voltage clamp (CA-1; Dagan Corporation) (Stefani et al., 1994). Electrical access to the cytoplasm was obtained by adding 0.1% saponin briefly to the lower chamber. The intracellular solution contained 110 mM K-glutamate, 1 mM EGTA, and 10 mM HEPES, pH 7.0. The extracellular solution in the upper and guard chambers contained 107 mM *N*-methylglucamine-methanesulfonate (NMG-MES), 2 mM Ca-$(MES)_2$, and 10 mM HEPES, pH 7.0 with or without 10 mM $MgCl_2$ as indicated. The intracellular recording electrode contained 2.7 M Na-MES, 10 mM NaCl, 1 mM EGTA, and 10 mM HEPES, pH 7.0. Agar bridges contained platinum wires and were filled with 1 M Na-MES. Capacitive and linear leak currents were compensated using the amplifier. For all cut-open oocyte clamp experiments, the membrane was held at −90 mV and pulsed in 3-mV increments to potentials ranging from −120 to 18 mV. Data were sampled at 20 kHz and filtered at 4 kHz. Pulse durations were varied as needed to accommodate differences in gating current kinetics in the W434F and mutant channels (see figure legends).

Gating current records were integrated to obtain the gating charge (Q) moved as a function of voltage. We verified that ON and OFF gating charges were equal (not depicted). Gating charge values were normalized to the maximum value obtained during the experiment and plotted versus voltage. Q-V data were fitted with the sum of two Boltzmann functions to obtain the midpoint potential ($V_{1/2}$) and apparent valence (z) values for the q1 and q2 components of gating charge movement (Bezanilla et al., 1994; Perozo et al., 1994; Baker et al., 1998).

The kinetics of charge movement were characterized by fitting ON gating currents with single-exponential functions to obtain values of ON gating current time constant (τ_{on}). Below −20 mV, two kinetic components of charge movement corresponding to q1 and q2 can be resolved in W434F channels using long (>100 ms) pulses (Bezanilla et al., 1994). Above −20 mV, the kinetics of q1 and q2 merge, and only one component can be resolved (Bezanilla et al., 1994). The slower, q2, component of charge movement could

not be detected in the I287D+F324D mutant used in this study because it activates significantly slower than the control channel. It is likely that the faster (q1) component of gating charge movement makes a major contribution to the single τ_{on} values measured at voltages below −20 mV (Bezanilla et al., 1994). At more positive voltages, the kinetics of the total charge movement are well represented by τ_{on}.

Structural modeling

Three-dimensional models of the voltage sensor domains of Shaker-IR and I287D+F324D were generated with the program Modeller using residues 160–307 of the Kv1.2/Kv2.1 voltage sensor paddle chimera x-ray structure (PDB accession number 2R9R) as the template (Eswar et al., 2006; Long et al., 2007). Sequences encompassing S1 through S4, corresponding to residues 160–307 and 224–378 in the chimera and Shaker, respectively, were aligned using ClustalW and manually optimized. To model Shaker containing the engineered Mg^{2+} binding site, I287 and F324 were mutated in silico to aspartate, a Mg^{2+} ion was manually positioned to achieve ideal bond distances (2.2–2.4 Å), and the model was subsequently idealized using the program Refmac (Collaborative Computation Project, Number 4, 1994).

RESULTS

Mg^{2+} does not alter activation or deactivation kinetics in Shaker-IR

Shaker-IR was expressed in *Xenopus* oocytes for voltage clamp analysis in the presence and absence of Mg^{2+} (Fig. 2). Ionic currents were elicited by stepping from −100 mV to voltages ranging from −60 to +90 mV in 10-mV increments (Fig. 2 A). The dependence of channel opening on voltage was determined from steady-state current amplitudes (Fig. 2 B). The addition of 10 mM Mg^{2+} shifted the g-V curve ∼12 mV in the depolarized direction (Fig. 2 B). This surface charge effect has been described previously and is known to be mediated by residues in the outer pore and the extracellular linker between S5 and the P loop (Elinder and Århem, 2003; Broomand et al., 2007).

To characterize Shaker-IR activation kinetics in the presence and absence of Mg^{2+}, current traces were fitted with a single-exponential function, providing values for the τ_{act} as a function of voltage (Fig. 2, C and D). In the presence of Mg^{2+}, the τ_{act}–voltage curve was shifted in the depolarized direction due to the surface charge effect of Mg^{2+}. After correcting for this shift, Mg^{2+} had no significant effect on Shaker activation kinetics (Fig. 2 D).

To determine whether Mg^{2+} altered deactivation kinetics, the membrane was stepped from −100 to +40 mV, followed by repolarization to voltages ranging from −50 to −125 mV in 5-mV increments. Tail currents were recorded in a bath solution containing 98 mM K^+. Tail current traces were fitted with a single-exponential component to obtain values for τ_{deact} as a function of repolarization potential (Fig. 2, E and F). After correcting for the surface charge effect, Mg^{2+} did not significantly change the deactivation kinetics of Shaker-IR channels (Fig. 2 F). We conclude that Shaker-IR is insensitive to Mg^{2+}.

Mg^{2+} increases the delay before pore opening and slows activation kinetics in I287D+F324D

In Shaker, positions 287 in S2 and 324 in S3b correspond to the aspartate residues that contribute to the divalent cation binding site in eag (Fig. 1 B) (Silverman et al., 2000). To determine whether a functional divalent cation binding site can be engineered into Shaker-IR, I287 and F324 were mutated to aspartate and the double-mutant protein was expressed in oocytes for voltage clamp analysis (Fig. 3 A). I287D+F324D shifted the g-V curve in the depolarized direction and reduced its apparent valence compared with Shaker-IR. The addition of extracellular Mg^{2+} shifted the g-V curve an additional +5 mV and increased its apparent valence (Fig. 3 B).

Current traces obtained in the presence and absence of Mg^{2+} were fitted with a single-exponential function, and values of τ_{act} were plotted versus voltage (Fig. 3 C). After correcting for the surface charge effect, activation kinetics were significantly slowed by Mg^{2+} over the entire voltage range tested, with two- to threefold increases in τ_{act} (Fig. 3 C).

In addition to slowing activation kinetics, Mg^{2+} also increased the delay before pore opening (Fig. 3, D and E). The delay was estimated by extrapolating the fitted exponential function to 0 current amplitude. The difference between this intercept and the start of the voltage pulse at $t = 0$ ms was measured as the delay for ionic current activation (Perozo et al., 1994). Delay values measured in the presence and absence of Mg^{2+} were plotted versus test potential (Fig. 3 E). Mg^{2+} significantly increased the delay at all analyzed voltages.

To characterize the deactivation kinetics of I287D+F324D in the presence and absence of Mg^{2+}, tail currents were recorded in a 98-mM K^+ bath solution (Fig. 3 F). After correcting for the surface charge effect, Mg^{2+} had no significant effect on τ_{deact} values (Fig. 3 G).

In eag, Mg^{2+} slows activation with little or no effect on the kinetics of deactivation (Tang et al., 2000). Therefore, mutating I287 and F324 in Shaker to aspartate generates a functional divalent cation binding site similar to the one in eag.

Acidic residues in S2 and S3 (but not E283) are required to confer Mg^{2+} sensitivity on Shaker activation

In eag, Mg^{2+} binding requires both acidic residues D278 in S2 and D327 in S3b (Fig. 1) (Silverman et al., 2000). To determine whether both aspartate mutations are needed for Mg^{2+} modulation of activation in Shaker, we investigated the Mg^{2+} sensitivity of the single mutants I287D and F324D. After correcting for the surface charge effect, neither activation nor deactivation kinetics were affected by extracellular Mg^{2+} in I287D or in F324D (Fig. 4, A–F). These results indicate that both positions must contain an acidic residue to generate a divalent cation binding site in the Shaker voltage sensor domain.

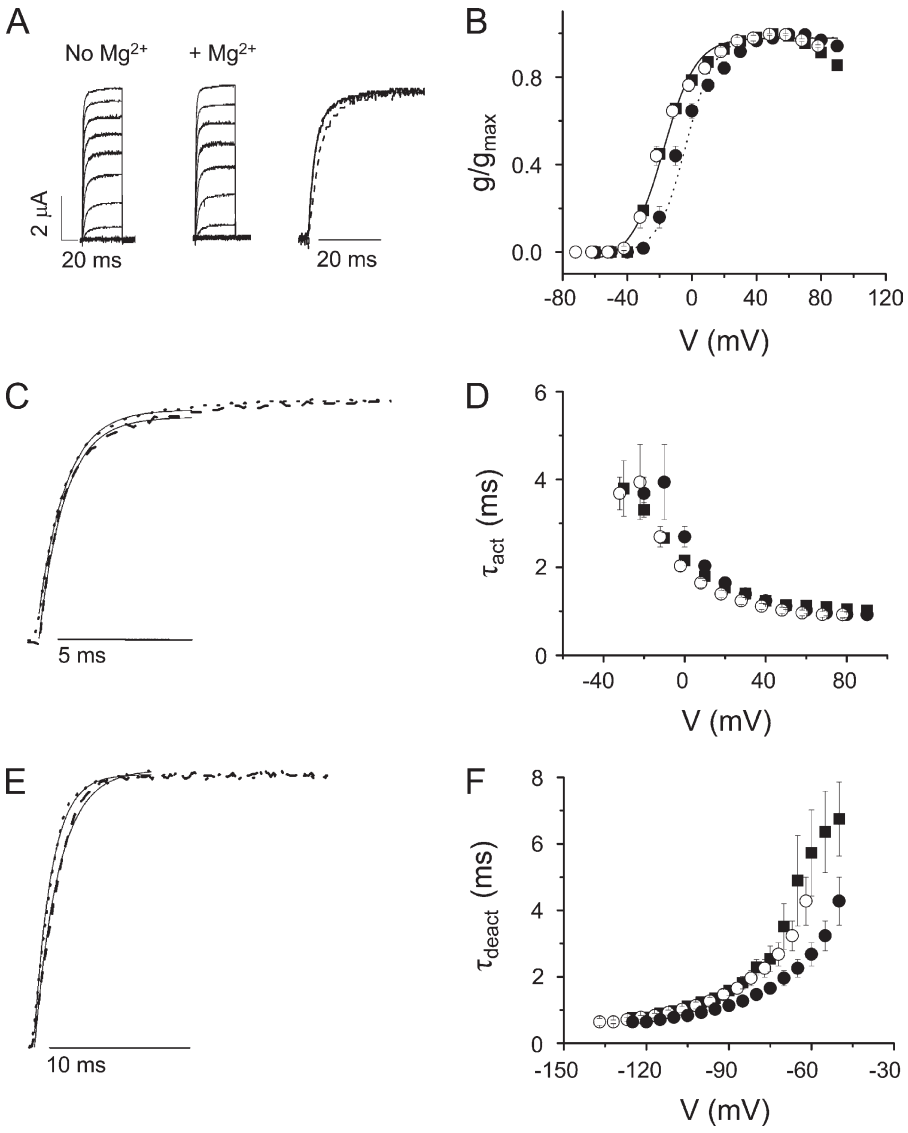

Figure 2. Shaker-IR is insensitive to extracellular Mg^{2+}. (A) Shaker-IR currents were recorded in the absence (left) or presence (middle) of 10 mM of extracellular Mg^{2+}. From a holding potential of −100 mV, 50-ms test pulses to voltages between −60 and +90 mV were applied in 10-mV increments. In this and subsequent figures, traces obtained by pulses ranging from −60 to +40 mV are shown. (Right) Currents recorded at −10 mV in the absence (solid trace) or presence (dashed) of Mg^{2+} have been scaled and overlaid. (B) Mg^{2+} shifts the voltage dependence of activation in Shaker-IR channels. Conductance values were calculated from steady-state current amplitudes during a 50-ms test pulse. Normalized conductance values (g/g_{max}) obtained in the absence (■) or presence (●) of Mg^{2+} were plotted versus voltage. Datasets were fitted with single Boltzmann functions. Values of $V_{1/2}$ in the absence and presence of Mg^{2+} were −19 ± 1 and −7 ± 2 mV, respectively. Values of the apparent valence were 2.5 ± 0.2 and 2.5 ± 0.1 without and with Mg^{2+}, respectively. To correct for the field effect of Mg^{2+}, g/g_{max} values obtained in Mg^{2+} were shifted by −12 mV and replotted (○). Data are provided as mean ± SEM; n = 6. (C) Current traces have been scaled and overlaid after approximate correction for the surface charge effect of Mg^{2+}. Representative current traces were recorded at +20 mV in the absence (dashed trace) or at +30 mV in the presence (dotted trace) of Mg^{2+}. Fitted exponential functions (solid lines) have been superimposed. Values of τ_{act} in the absence (+20 mV) or presence (+30 mV) of Mg^{2+} were 1.2 ± 0.1 and 1.1 ± 0.1 ms, respectively, and did not differ significantly ($P \geq 0.05$). (D) Activation kinetics are unaffected by Mg^{2+}. τ_{act} in the absence (■) or presence (●) of Mg^{2+} were obtained by fitting single-exponential functions to the current traces and plotted versus voltage. To correct for the field effect of Mg^{2+}, τ_{act} values obtained in Mg^{2+} were shifted by −12 mV and replotted (○). Data are shown as mean ± SEM; n = 6. (E) Tail current traces have been scaled and overlaid after approximate correction for the surface charge effect of Mg^{2+}. Representative tail currents were recorded at −100 mV in the absence (dashed trace) or at −90 mV in the presence (dotted trace) of Mg^{2+}. Fitted exponential functions (solid lines) have been superimposed. The values of τ_{deact} in the absence (−100 mV) and presence (−90 mV) of Mg^{2+} did not differ significantly and were 1.4 ± 0.1 and 1.5 ± 0.1 ms, respectively. (F) Mg^{2+} does not affect deactivation kinetics. The membrane was depolarized to +40 mV, followed by repolarization to tail potentials ranging from −50 to −125 mV. Tail currents recorded in the absence (■) or presence (●) of Mg^{2+} were fitted with a single-exponential component to obtain values for τ_{deact}, which were plotted versus repolarization voltage. Data are provided as mean ± SEM; n = 9. To correct for the field effect of Mg^{2+}, values of τ_{deact} obtained in the presence of Mg^{2+} were shifted by −12 mV and replotted (○).

In eag, the widely conserved acidic residue (D274) near the extracellular end of S2 is not required for Mg^{2+} binding, although its side chain does project into the same external gating crevice that contains the binding site (Fig. 1) (Silverman et al., 2000). To determine whether the analogous acidic residue in Shaker, E283, contributes to ion binding in the I287D+F324D mutant channel, we investigated the Mg^{2+} sensitivity of a triple mutant channel in which E283 was replaced by the neutral residue, alanine (Fig. 5).

Currents were recorded from E283A+I287D+F324D channels in the presence and absence of Mg^{2+} (Fig. 5 A). Similarly to I287D+F324D, the triple mutant shifted the g-V curve in the depolarized direction and reduced its apparent valence compared with Shaker-IR. The addition of extracellular Mg^{2+} shifted the g-V curve an additional +8 mV (Fig. 5 B).

After correcting for the surface charge effect, extracellular Mg^{2+} significantly slowed activation in E283A+I287D+F324D throughout the entire voltage range tested,

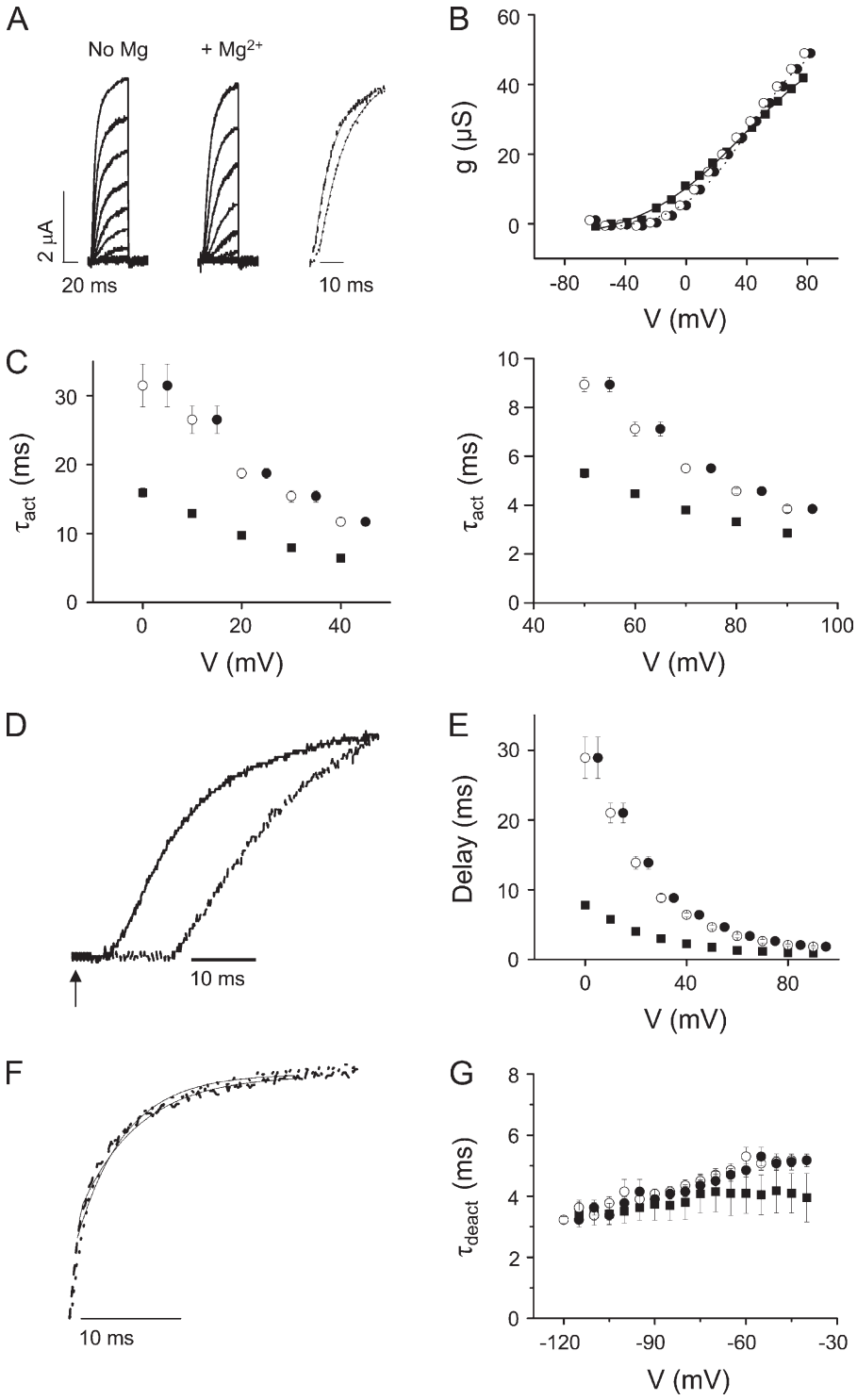

Figure 3. Mg^{2+} significantly slows activation and increases the delay before pore opening in I287D+F324D channels. (A) I287D+F324D currents were recorded in the absence (left) or presence (middle) of Mg^{2+}. (Right) After approximate correction for the nonspecific field effect of Mg^{2+} (see B), current traces have been scaled and overlaid. Representative current traces were recorded at +20 mV in the absence (dashed trace) or at +30 mV in the presence (dotted trace) of Mg^{2+}. Fitted exponential functions (solid lines) have been superimposed. (B) Mg^{2+} shifts the voltage dependence of activation in I287D+F324D channels. Because the conductance of I287D+F324D channels did not saturate in the tested voltage range, un-normalized conductance values from a representative experiment are shown. Data were obtained in the absence (■) or presence (●) of Mg^{2+}, plotted versus voltage, and fitted with a single Boltzmann function without constraining the maximum conductance value. Fitted parameters from individual experiments were averaged and are provided as mean ± SEM; $n = 8$. Values of $V_{1/2}$ and apparent valence in the absence and presence of Mg^{2+} were 38 ± 2 mV and 0.7 ± 0.04, and 43 ± 1 mV and 1.0 ± 0.07, respectively. To correct for the field effect of Mg^{2+}, conductance values obtained in Mg^{2+} were shifted by −5 mV and

indicating that an acidic residue at position 283 is not required for ion binding (Fig. 5 C). Mg^{2+} also increased the delay before activation of the ionic conductance (Fig. 5, D and E). Deactivation kinetics of E283A+I287D+F324D were not significantly affected by extracellular Mg^{2+} (not depicted).

Mg^{2+} and H^+ compete for the ion binding site in Shaker voltage sensor

Having two negatively charged amino acid residues in sufficient proximity to generate an ion binding site is likely to affect the pKa values of their side chain carboxylate groups. In free solution, the pKa of the side chain carboxylic acid moiety in aspartate is ~3.9. To determine whether this value is altered in the I287D+F324D mutant, we tested the Mg^{2+} sensitivity of Shaker activation kinetics at pH 5.5, 6.5, 7.5, and 8.0 (Fig. 6). We found that Mg^{2+} was less effective at slowing activation kinetics at pH 6.5 than at 7.5 or 8.0, and that Mg^{2+} had no significant effect on activation kinetics at pH 5.5 (Fig. 6, A and B). We also varied the pH and investigated the effect of Mg^{2+} on the delay before pore opening. Mg^{2+} was less effective at lengthening the delay at pH 6.5 than at 7.5 or 8.0, and had no significant effect on the delay at pH 5.5 (Fig. 6, A and C). We conclude that the pKa of the side chain carboxylate in aspartate is significantly higher at the ion binding site than in solution.

At pH 5.5, activation was slow (similar to Mg^{2+}-bound kinetics) and the delay was long, whether or not extracellular Mg^{2+} was present (Fig. 6). These results indicate that neutralization of the aspartate residues by protonation or, presumably, charge shielding by bound Mg^{2+} increases the delay and slows opening in the Shaker I287D+F324D mutant channel.

To determine whether the nearby acidic residue E283 influences the pKa of the aspartate residues in the binding site, we investigated the effect of pH on the delay before pore opening and on ionic current kinetics in E283A+I287D+F324D channels in the presence and absence of Mg^{2+} (Fig. 7 A). As in I287D+F324D, Mg^{2+} slowed activation kinetics and increased the delay less effectively at pH 6.5 than at 7.5 or 8.0 (Fig. 7, B and C). Mg^{2+} had no significant effect on the delay or rate of pore opening at pH 5.5 (Fig. 7, B and C). At low pH, activation was slow and the delay was long, whether or not Mg^{2+} was present (Fig. 7). These results indicate that E283 does not contribute significantly to the shift in side chain pKa of aspartate residues in the binding site.

Mg^{2+} shifts the voltage dependence and slows the kinetics of gating charge movement in I287D+F324D

The finding that Mg^{2+} increases the delay before pore opening in I287D+F324D channels strongly suggests that the ion binds to the resting voltage sensor conformation. We tested this conclusion by recording gating currents, which provide a direct electrical measurement of voltage sensor conformational changes, in the presence and absence of extracellular Mg^{2+}. For gating current experiments, the W434F mutation was inserted into the Shaker sequence to block ionic conductance (Perozo et al., 1993).

Shaker gating currents consist of two components of charge movement, q1 and q2 (Bezanilla et al., 1994; Perozo et al., 1994; Baker et al., 1998). The q1 component moves at more hyperpolarized voltages than q2 and therefore represents the initial voltage-dependent transitions in the activation pathway. The q1 component is not rate limiting for activation; at the ionic current level, transitions in the q1 phase are responsible for the delay that precedes pore opening (Bezanilla et al., 1994; Perozo et al., 1994). The q2 component has a voltage dependence similar to that of channel opening and represents transitions between closed states late in the activation pathway. Movement of the q2 charge

replotted (○). (C) Mg^{2+} slows activation kinetics in I287D+F324D. (Left) Values of τ_{act} obtained in the absence (■) or presence (●) of Mg^{2+} have been plotted versus voltage from 0 to +45 mV. To correct for the field effect of Mg^{2+}, τ_{act} values obtained in Mg^{2+} were shifted by −5 mV and replotted (○). Data are provided as mean ± SEM; $n = 7$. Shifted τ_{act} values obtained with Mg^{2+} and τ_{act} values obtained without Mg^{2+} differed significantly; $P < 0.05$. (Right) Values of τ_{act} obtained at voltages from +50 to +95 mV are shown on an expanded scale; symbols as described above. To correct for the field effect of Mg^{2+}, τ_{act} values obtained in Mg^{2+} were shifted by −5 mV and replotted (○). Shifted τ_{act} values obtained with Mg^{2+} and τ_{act} values obtained without Mg^{2+} differed significantly; $P < 0.05$. (D) Representative current traces recorded at +20 mV in the absence (solid trace) or at +25 mV in the presence (dashed trace) of Mg^{2+} are shown on an expanded time scale to highlight the delay before pore opening. The arrow indicates start of voltage pulse ($t = 0$). Values of τ_{act} obtained in the absence (+20 mV) and presence (+25 mV) of Mg^{2+} differed significantly and were 9.9 ± 0.3 and 20.2 ± 0.5 ms, respectively ($n = 7$; $P < 0.05$). Measured delay values were 4.6 ± 0.2 ms at +20 mV in the absence and 11.3 ± 0.8 ms at +25 mV in the presence of Mg^{2+} ($n = 7$; $P < 0.05$). (E) Mg^{2+} increases the delay before activation of the ionic conductance in I287D+F324D. The delay before pore opening was measured in the absence (■) or presence (●) of Mg^{2+} and plotted versus voltage. Data are provided as mean ± SEM; $n = 10$. To correct for the field effect of Mg^{2+}, delays measured in the presence of Mg^{2+} were shifted by −5 mV and replotted (○). Shifted delay values obtained with Mg^{2+} and delay values obtained without Mg^{2+} differed significantly; $P < 0.05$. (F) Mg^{2+} does not affect deactivation kinetics. Representative tail currents evoked at −95 mV in the absence (dashed trace) or at −90 mV in the presence (dotted trace) of Mg^{2+} have been scaled and overlaid. Values of τ_{deact} in the absence (−95 mV) and presence (−90 mV) of Mg^{2+} were 3.7 ± 0.5 and 3.9 ± 0.1 ms, respectively, and did not differ significantly. (G) The membrane was depolarized to +40 mV, followed by repolarization for 200 ms to tail potentials ranging from −40 to −115 mV. Tail current traces were fitted with single-exponential functions to obtain values for τ_{deact} in the absence (■) or presence (●) of Mg^{2+}, which were plotted versus repolarization voltage. Data are provided as mean ± SEM; $n = 4$. To correct for the field effect of Mg^{2+}, τ_{deact} values obtained in Mg^{2+} were shifted by −5 mV and replotted (○).

component is the rate-determining step in Shaker activation (Bezanilla et al., 1994).

Gating currents were recorded from control (W434F), I287D+F324D, and I287D channels using a cut-open oocyte voltage clamp (Fig. 8, A–C). Although gating currents could be detected in F324D channels, they were extremely small in amplitude and were not studied further (not depicted). To compare gating charge movement in the presence and absence of Mg^{2+}, ON gating currents were integrated to obtain the gating charge, Q, which was normalized to the maximum value obtained in the experiment and plotted versus voltage (Fig. 8). The data were fitted with the sum of two Boltzmann functions to obtain values for the midpoint voltage ($V_{1/2}$) and apparent valence (z) for the q1 (V_1, z_1) and q2 (V_2, z_2) components of charge movement (Table I).

In the absence of Mg^{2+}, the q1 charge component in I287D+F324D channels had a similar $V_{1/2}$ value but a twofold lower apparent valence compared with control channels (Table I). The q2 component was shifted in the depolarized direction, and its apparent valence was also reduced. In contrast, the q1 and q2 components in I287D channels were shifted in the hyperpolarized direction compared with control. Although z_1 was similar to that of the control channel, z_2 was reduced (Table I).

The addition of Mg^{2+} significantly altered the steady-state properties of gating currents in I287D+F324D, but not in control or I287D channels (Fig. 8 and Table I). In the presence of Mg^{2+}, the q1 and q2 components of charge movement in I287D+F324D were significantly shifted in the depolarized direction. In addition, the apparent valence of the q1 component (z_1) increased to the value seen in the control channel with or without Mg^{2+}. In contrast to its effect on the g-V curve, Mg^{2+} did not shift the Q-V curves of the control or I287D channels. Similarly, their z_1 and z_2 valences were unaffected by Mg^{2+}.

In W434F channels, two kinetic components of charge movement are associated with the q1 and q2 phases of the activation mechanism (Bezanilla et al., 1994). Below

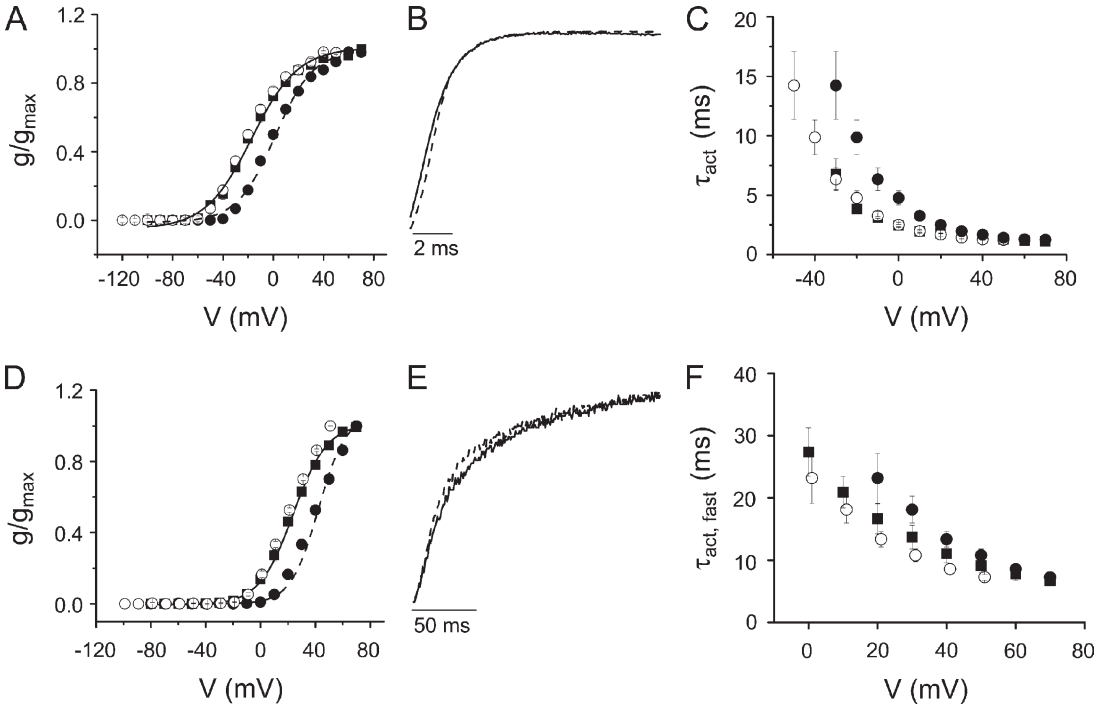

Figure 4. Single mutants I287D (A–C) and F324D (D–F) are insensitive to extracellular Mg^{2+}. (A and D) Mg^{2+} shifts the voltage dependence of activation in (A) I287D and (D) F324D channels. Values of g/g_{max} obtained in the absence (■) or presence (●) of Mg^{2+} were plotted versus voltage. Data are provided as mean ± SEM; $n = 6$ (I287D) or 8–9 (F324D). Data were fitted with a single Boltzmann function. Values of $V_{1/2}$ and apparent valence for I287D in the absence and presence of Mg^{2+} were −20 ± 2 mV and 1.7 ± 0.1, and 0 ± 1 mV and 1.5 ± 0.2, respectively. Values of $V_{1/2}$ and apparent valence for F324D in the absence and presence of Mg^{2+} were 21 ± 1 mV and 2.1 ± 0.2, and 40 ± 1 mV and 2.5 ± 0.3, respectively. To correct for the field effect of Mg^{2+}, g/g_{max} values obtained in Mg^{2+} were shifted by −20 mV and replotted (○). (B and E) Representative I287D (B) and F324D (E) currents recorded at +20 mV in the absence (solid trace) and +40 mV in the presence (dashed trace) of Mg^{2+} have been scaled and overlaid. Values of τ_{act} (I287D) or $\tau_{act,fast}$ (F324D) obtained in the absence (+20 mV) and presence (+40 mV) of Mg^{2+} did not differ significantly and were 2 ± 0.1 and 2 ± 0.1 ms for I287D, and 17 ± 2 and 14 ± 1 ms for F324D, respectively. (C and F) Mg^{2+} does not affect activation kinetics in (C) I287D or (F) F324D. I287D and F324D current traces recorded in the absence (■) or presence (●) of Mg^{2+} were fitted with single- (I287D) or double- (F324D) exponential functions. Values of τ_{act} were plotted versus voltage. In F, only the major, fast kinetic component of F324D activation is shown. Data are shown as mean ± SEM; $n = 6$ (I287D) or 3 (F324D). To correct for the field effect of Mg^{2+}, τ_{act} values obtained in Mg^{2+} were shifted by −20 mV and replotted (○).

−20 mV, movement of q2 is significantly slower than q1; long pulses (>100 ms) are required to characterize the q2 kinetic component (Bezanilla et al., 1994). In I287D+F324D, the slower q2 component could not be detected, reflecting the fact that activation is significantly slower in I287D+F324D than in control channels (Figs. 2 D and 3 C). Therefore, we characterized gating current kinetics in the presence and absence of Mg^{2+} by fitting ON gating currents with a single-exponential function to obtain values for τ_{on} (Fig. 9). Previously reported results obtained with W434F channels suggest that the fast q1 phase of charge movement makes a major contribution to τ_{on} values measured at hyperpolarized voltages. We obtained a value of 3.0 ± 0.3 ms for τ_{on} in the control channel at −39 mV. For comparison, time constants for the fast q1 and slow q2 components

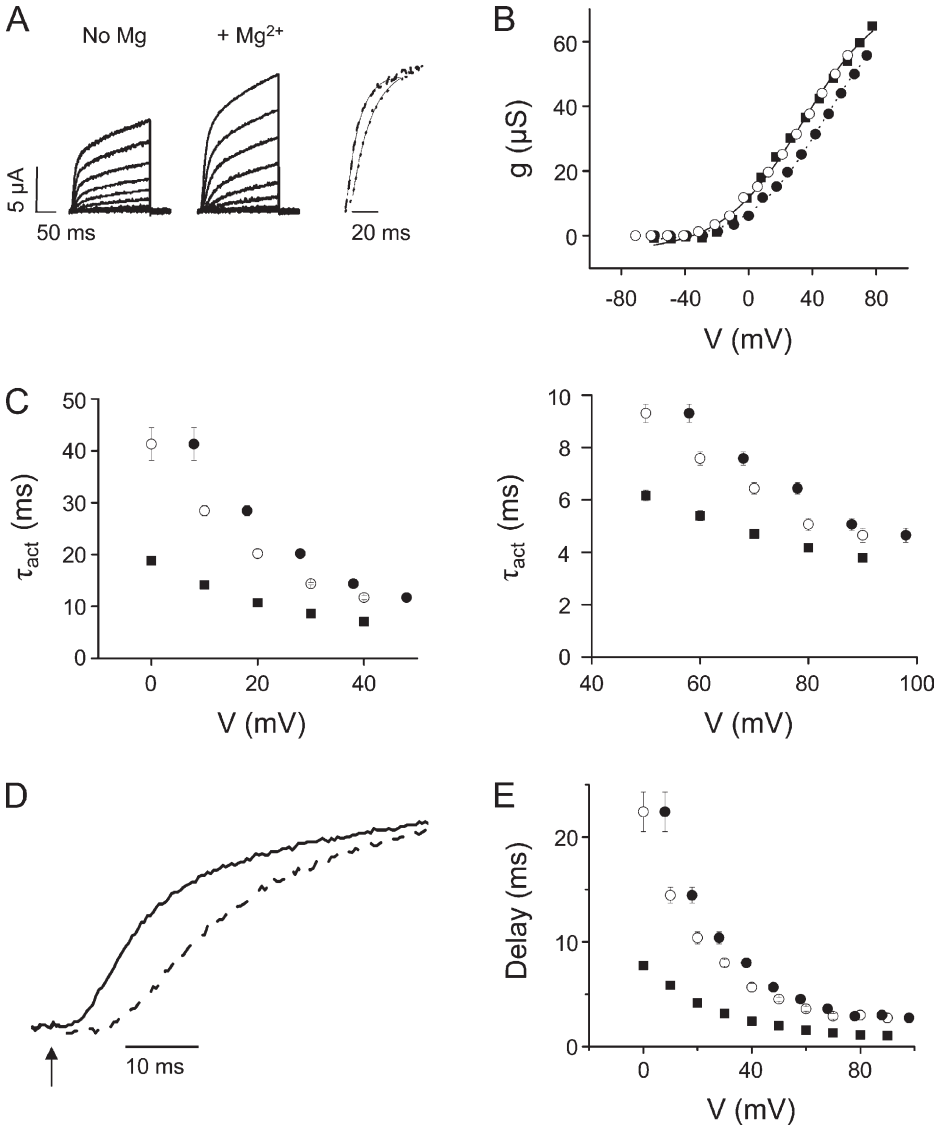

Figure 5. E283 is not required for Mg^{2+} modulation of activation time course in I287D+F324D. (A) E283A+I287D+F324D currents were recorded in the absence (left) or presence (middle) of Mg^{2+}. (Right) After approximate correction for the nonspecific field effect of Mg^{2+} (see B), representative current traces recorded at +20 mV in the absence (dashed trace) or at +30 mV in the presence (dotted trace) of Mg^{2+} have been scaled and overlaid. Single-exponential fits to the data are shown (solid curves). (B) Mg^{2+} shifts the voltage dependence of activation in E283A+I287D+F324D. Because the conductance of E283A+I287D+F324D channels did not saturate in the tested voltage range, un-normalized conductance values from a representative experiment are shown. Data were obtained in the absence (■) or presence (●) of Mg^{2+}, plotted versus voltage, and fitted with a single Boltzmann function without constraining the maximum conductance value. Fitted parameters from individual experiments were averaged and are provided as mean ± SEM; $n = 8$. Values of $V_{1/2}$ and apparent valence in the absence and presence of Mg^{2+} were 36 ± 3 mV and 0.8 ± 0.07, and 44 ± 4 mV and 0.9 ± 0.07, respectively. To correct for the field effect of Mg^{2+}, conductance values obtained in Mg^{2+} were shifted by −8 mV and replotted (○). (C) Mg^{2+} slows activation kinetics. (Left) Values of τ_{act} obtained in the absence (■) or presence (●) of Mg^{2+} have been plotted versus voltage from 0 to +48 mV. Data are provided as mean ± SEM; $n = 8$. To correct for the field effect of Mg^{2+}, τ_{act} values obtained in Mg^{2+} were shifted by −8 mV and replotted (○). Shifted τ_{act} values obtained with Mg^{2+} and τ_{act} values obtained without Mg^{2+} differed significantly; $P < 0.05$. (Right) Values of τ_{act} obtained at voltages from +50 to +98 mV are shown on an expanded scale; symbols as described above. To correct for the field effect of Mg^{2+}, τ_{act} values obtained in Mg^{2+} were shifted by −8 mV and replotted (○). Shifted τ_{act} values obtained with Mg^{2+} and τ_{act} values obtained without Mg^{2+} differed significantly; $P < 0.05$. (D) Representative current traces recorded at +20 mV in the absence (solid trace) or at +28 mV in the presence (dashed trace) of Mg^{2+} are shown on an expanded time scale to highlight the delay before pore opening. The arrow indicates start of voltage pulse ($t = 0$). Values of τ_{act} measured in the absence (+20 mV) and presence (+28 mV) of Mg^{2+} were 11.3 ± 0.5 and 18.5 ± 1.2 ms, respectively, and differed significantly ($P < 0.05$; $n = 8$). Measured delay values were 3.3 ± 0.3 ms at +20 mV in the absence and 9.1 ± 0.2 ms at +28 mV in the presence of Mg^{2+} and differed significantly ($P < 0.05$; $n = 8$). (E) Mg^{2+} increases the delay before activation of the ionic conductance in E283A+I287D+F324D. The delay before pore opening was measured in the absence (■) or presence (●) of Mg^{2+} and plotted versus voltage. Data are provided as mean ± SEM; $n = 10$. To correct for the field effect of Mg^{2+}, delays measured in the presence of Mg^{2+} were shifted by −8 mV and replotted (○). Shifted delay values obtained with Mg^{2+} and delay values obtained without Mg^{2+} differed significantly; $P < 0.05$.

TABLE I

Steady-state gating current parameters in the presence and absence of Mg^{2+}

Construct	V_1		z_1		V_2		z_2		n
	no Mg^{2+}	+Mg^{2+}	no Mg^{2+}	+Mg^{2+}	no Mg^{2+}	+Mg^{2+}	no Mg^{2+}	+Mg^{2+}	
	mV				*mV*				
I287D+F324D+W434F	−61 ± 1	−53 ± 1[a]	1.4 ± 0.1	2.7 ± 0.5[a]	−26 ± 1	−16 ± 1[a]	3.0 ± 0.1	2.8 ± 0.4	7
I287D+W434F	−78 ± 2	−78 ± 1	2.2 ± 0.5	2.5 ± 0.3	−60 ± 1	−60 ± 0.2	3.1 ± 0.4	3.5 ± 0.3	6
W434F	−61 ± 2	−60 ± 2	2.8 ± 0.1	2.7 ± 0.1	−40 ± 1	−37 ± 1	5.6 ± 0.3	5.3 ± 0.2	8

Normalized gating charge was plotted versus voltage, and data were fitted with the sum of two Boltzmann functions to obtain values for $V_{1/2}$ and valence (z). Parameters for q1 component of gating charge: V_1 and z_1. Parameters for q2 component of gating charge: V_2 and z_2. Values are provided as mean ± SEM. [a]Significantly different from value obtained in the absence of Mg^{2+}; $P < 0.05$ by ANOVA.

of charge movement in W434F channels at −40 mV have been reported to be ~1.75 and ~15 ms, respectively (Bezanilla et al., 1994). At more positive voltages, the kinetics of q1 and q2 merge and the total charge movement is well described by a single-exponential function (Bezanilla et al., 1994).

Mg^{2+} slowed gating current kinetics and shifted the voltage dependence of τ_{on} in I287D+F324D, but not in I287D or control channels (Fig. 9, A–C, and Table II). In I287D+F324D channels, Mg^{2+} shifted τ_{on} values in the depolarized direction throughout the tested voltage range, consistent with the effect of Mg^{2+} on the voltage dependence of gating charge movement (Figs. 8 and 9). At potentials more positive than −24 mV, corresponding to voltages that open I287D+F324D channels, Mg^{2+} significantly increased the value of τ_{on}. In contrast, Mg^{2+} had no significant effects on the value or voltage dependence of τ_{on} in I287D or control channels (Fig. 9 and Table II).

DISCUSSION

In I287D+F324D, Mg^{2+} binds to the resting conformation of the voltage sensor domain

We have engineered a divalent cation binding site in the Shaker voltage sensor domain by simultaneously mutating I287 in S2 and F324 in S3b to aspartate. Our data

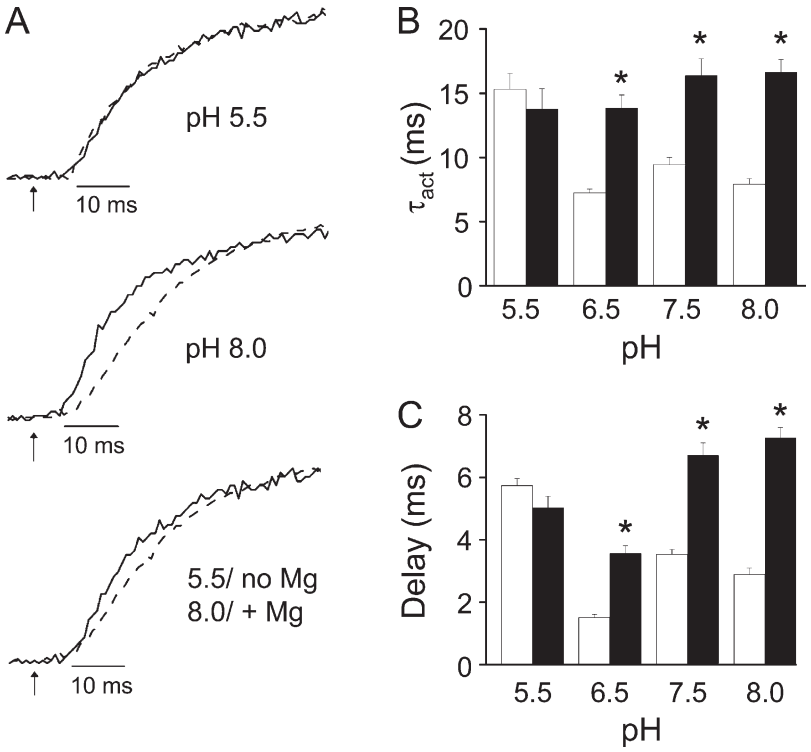

Figure 6. Low pH abolishes Mg^{2+} modulation of delay and activation kinetics in I287D+F324D channels. (A) Representative currents recorded at pH 5.5 (top) or pH 8.0 (middle) at +20 mV in the absence (solid trace) or at +30 mV (+20 mV at pH 5.5 only) in the presence (dashed trace) of Mg^{2+} have been scaled and overlaid. (Bottom) Representative currents recorded at pH 5.5 in the absence of Mg^{2+} (solid trace; +20 mV) or at pH 8.0 in the presence of Mg^{2+} (dashed trace; +30 mV) have been scaled and overlaid. Arrows indicate start of voltage pulse ($t = 0$). (B) Bar graph shows τ_{act} values measured at pH 5.5, 6.5, 7.5, or 8.0 in the absence (open bars; +20 mV) or presence (filled bars; +30 mV, except for +20 mV at pH 5.5) of Mg^{2+}. Data are provided as mean ± SEM; n = 8–11. Asterisk (*), τ_{act} values measured in the presence and absence of Mg^{2+} differ significantly; $P < 0.05$ by ANOVA. Values of τ_{act} for I287D+F324D in the absence of Mg^{2+} were 15 ± 1 ms (pH 5.5), 7 ± 0.3 ms (pH 6.5), 9 ± 1 ms (pH 7.5), and 8 ± 0.4 ms (pH 8). Values of τ_{act} for I287D+F324D in the presence of Mg^{2+} were 14 ± 2 ms (pH 5.5), 14 ± 1 ms (pH 6.5), 16 ± 1 ms (pH 7.5), and 17 ± 1 ms (pH 8). (C) Bar graph shows delay before pore opening measured at pH 5.5, 6.5, 7.5, or 8.0 in the absence (open bars; +20 mV) or presence (filled bars; +30 mV, except for +20 mV at pH 5.5) of Mg^{2+}. Data are provided as mean ± SEM; n = 9–15. Asterisk (*), delay values measured in the presence and absence of Mg^{2+} differ significantly; $P < 0.05$ by ANOVA. Values of the delay for I287D+F324D in the absence of Mg^{2+} were: pH 5.5, 5.7 ± 0.2 ms; pH 6.5, 1.5 ± 0.1 ms; pH 7.5, 3.5 ± 0.2 ms; pH 8.0, 2.9 ± 0.2 ms. Values of the delay for I287D+F324D in the presence of Mg^{2+} were: pH 5.5, 5.0 ± 0.4 ms; pH 6.5, 3.6 ± 0.2 ms; pH 7.5, 6.7 ± 0.4 ms; pH 8.0, 7.3 ± 0.3 ms.

indicate that Mg^{2+} binds to the resting voltage sensor conformation to modulate activation gating. This conclusion is strongly supported by the results of ionic and gating current experiments. In I287D+F324D channels, Mg^{2+} significantly increased the delay before activation of the ionic conductance. This delay is due to the q1 phase of voltage sensor conformational changes, which corresponds to the initial transitions in the activation pathway (Bezanilla et al., 1994; Perozo et al., 1994). At the gating current level, Mg^{2+} shifted the voltage dependence of the q1 component in the depolarized direction. Shifting q1 transitions to more positive voltages increases the delay before pore opening by increasing the fraction of channels residing in deep closed states at the holding potential. Mg^{2+} also increased the apparent valence, z1, of the q1 charge component, consistent with the finding that Mg^{2+} increased the steepness of the I287D+F324D g-V curve.

Our results also indicate that Mg^{2+} remains bound to the I287D+F324D voltage sensor domain during the q2 phase of activation. Mg^{2+} slowed the rate of pore opening, increasing τ_{act} two- to threefold. This indicates that Mg^{2+} modulates the rate-determining step in Shaker activation, which corresponds to movement of the q2 component of gating charge (Bezanilla et al., 1994). Consistent with this observation, Mg^{2+} significantly slowed gating current kinetics at potentials that open the channel. In this voltage range, the kinetics of q1 and q2 charge movement overlap and are well described by the τ_{on} values measured in our experiments (Bezanilla et al., 1994). In addition, Mg^{2+} shifted the voltage dependence of q2 charge movement in the depolarized direction.

In contrast to I287D+F324D channels, Mg^{2+} did not significantly change the delay before pore opening or the kinetics of opening in control (Shaker-IR) channels or in the single mutants I287D or F324D. Similarly, Mg^{2+} had no effect on the steady-state or kinetic properties of gating currents in control (W434F) or I287D channels.

TABLE II

Gating current kinetics in the presence and absence of Mg^{2+}

Construct	τ_{on}, no Mg^{2+}	τ_{on}, + Mg^{2+}	*n*
	ms	*ms*	
I287D+F324D+W434F	10.2 ± 0.8	13.4 ± 0.6[a]	7
I287D+W434F	2.0 ± 0.2	2.4 ± 0.3	6
W434F	2.2 ± 0.1	2.3 ± 0.1	9

ON gating current traces recorded at −9 mV were fitted with a single exponential component to obtain values for τ_{on}, shown as mean ± SEM.
[a]Significantly different from value obtained in the absence of Mg^{2+}; $P < 0.05$ by ANOVA.

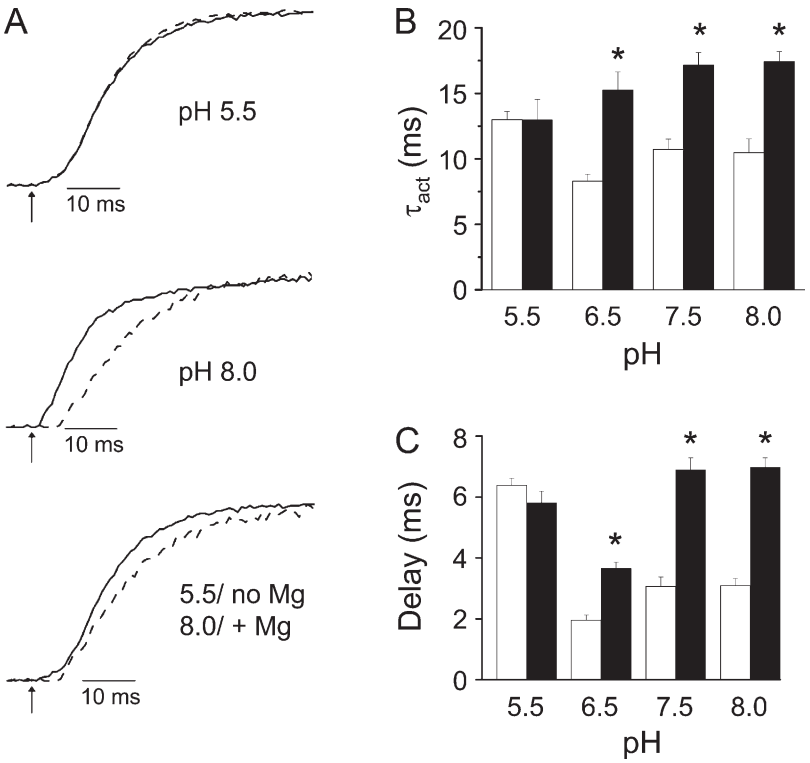

Figure 7. Low pH abolishes Mg^{2+} modulation of activation kinetics in E283A+I287D+F324D channels. (A) Representative currents recorded at pH 5.5 (top) or pH 8.0 (middle) at +20 mV in the absence (solid trace) or at +30 in the presence (+20 mV at pH 5.5 only) (dashed trace) of Mg^{2+} have been scaled and overlaid. (Bottom) Representative currents recorded at pH 5.5 in the absence of Mg^{2+} (solid trace; +20 mV) or at pH 8.0 in the presence of Mg^{2+} (dashed trace; +30 mV) have been scaled and overlaid. Arrows indicate start of voltage pulse ($t = 0$). (B) Bar graph shows τ_{act} values measured at pH 5.5, 6.5, 7.5, or 8.0 in the absence (open bars; +20 mV) or presence (filled bars; +30 mV, except for +20 mV at pH 5.5) of Mg^{2+}. Data are provided as mean ± SEM; $n = 8$–11. Asterisk (*), τ_{act} values measured in the presence and absence of Mg^{2+} differ significantly; $P < 0.05$ by ANOVA. Values of τ_{act} for E283A+I287D+F324D in the absence of Mg^{2+} were 13 ± 1 ms (pH 5.5), 8 ± 1 ms (pH 6.5), 11 ± 1 ms (pH 7.5), and 10 ± 1 ms (pH 8). Values of τ_{act} for E283A+I287D+F324D in the presence of Mg^{2+} were 13 ± 2 ms (pH 5.5), 15 ± 1 ms (pH 6.5), 17 ± 1 ms (pH 7.5), and 17 ± 1 ms (pH 8). (C) Bar graph shows delay before pore opening measured at pH 5.5, 6.5, 7.5, or 8.0 in the absence (open bars; +20 mV) or presence (filled bars; +30 mV, except for +20 mV at pH 5.5) of Mg^{2+}. Data are provided as mean ± SEM; $n = 8$–14. Asterisk (*), delay values measured in the presence and absence of Mg^{2+} differ significantly; $P < 0.05$ by ANOVA. Values of the delay for E283A+I287D+F324D in the absence of Mg^{2+} were: pH 5.5, 6.4 ± 0.2 ms; pH 6.5, 2.0 ± 0.2 ms; pH 7.5, 3.1 ± 0.3 ms; pH 8.0, 3.1 ± 0.2 ms. Values of the delay for E283A+I287D+F324D in the presence of Mg^{2+} were: pH 5.5, 5.8 ± 0.4 ms; pH 6.5, 3.7 ± 0.2 ms; pH 7.5, 6.9 ± 0.4 ms; pH 8.0, 7.0 ± 0.3 ms.

Our results provide a novel, short-range constraint on the structure of the resting voltage sensor domain. Formation of an ion binding site between positions 287 in S2 and 324 in S3b indicates that these positions are in atomic proximity (≤4 Å) in the resting conformation (Dokmanić et al., 2008). In I287D+F324D, Mg^{2+} modulates both phases of gating charge movement, indicating that the ion binding site persists during the major voltage-dependent conformational changes of activation. The binding site residues are also closely apposed (∼4 Å apart) at 0 mV, as indicated by the x-ray structure of the Kv1.2/Kv2.1 chimera (Long et al., 2007). Collectively, these data strongly suggest that I287 in S2 and F324 in S3b are within atomic proximity of one another in all voltage sensor conformations. We do not mean to imply that these residues are completely immobile during activation. Rather, the evidence is consistent with the conclusion that they remain within ∼3–5 Å of one another.

Mg^{2+} differentially affects the steady-state properties of charge movement and pore opening

Interestingly, Mg^{2+} shifted the voltage dependence of pore opening in all the constructs studied in our experiments, but shifted the voltage dependence of gating charge movement exclusively in I287D+F324D channels. These results suggest that the surface charge effect of Mg^{2+} at the ionic current level modifies pore opening, a weakly voltage-dependent step, but, in the absence of

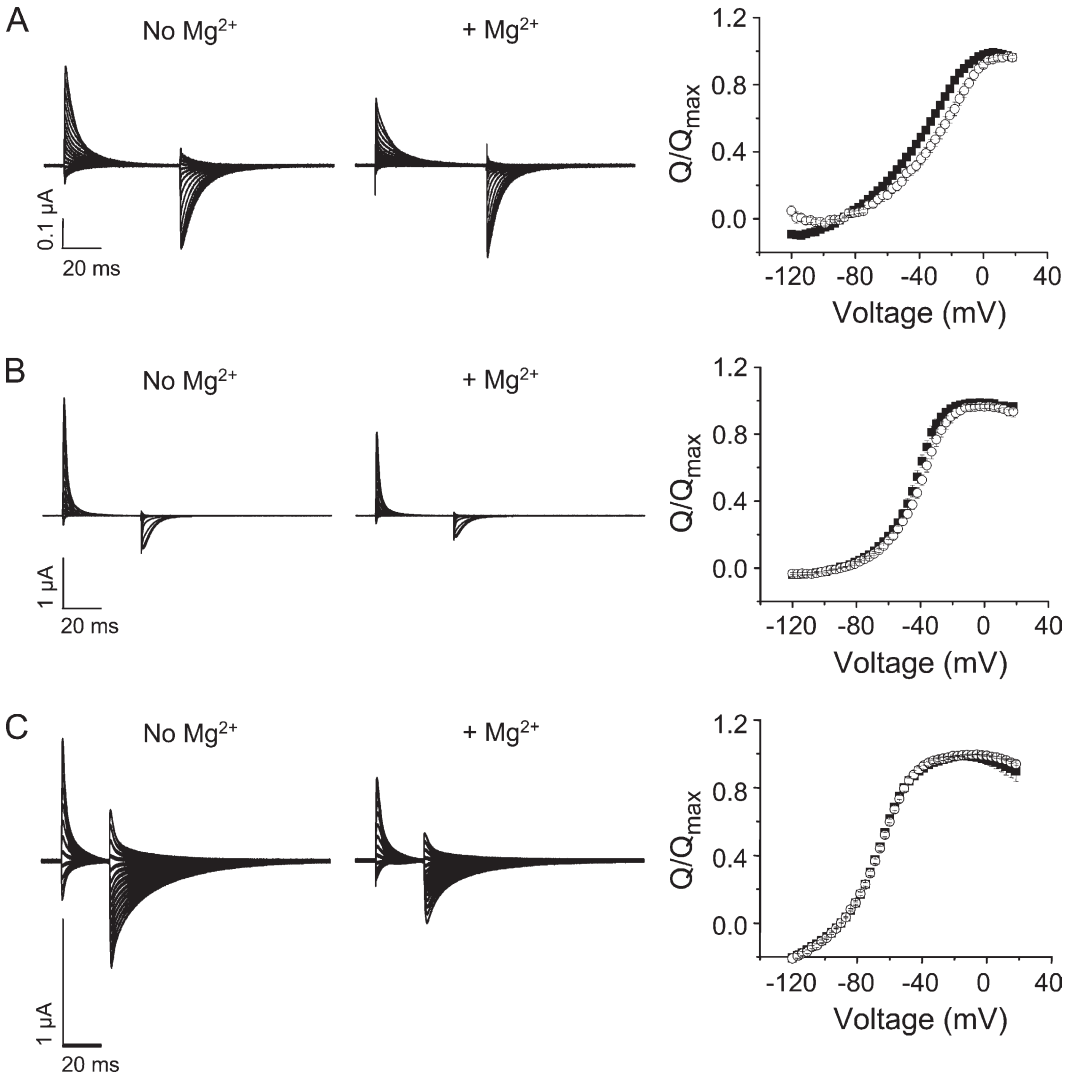

Figure 8. Mg^{2+} shifts the voltage dependence of gating charge movement in I287D+F324D channels, but not in control (W434F) or I287D channels. Gating currents were recorded from (A) I287D+F324D, (B) W434F, or (C) I287D channels in the absence (left) or presence (middle) of Mg^{2+}. From a holding potential of −90 mV, 60-ms (A), 40-ms (B), or 25-ms (C) test pulses to voltages between −120 and +18 mV were applied in 3-mV increments. Every third pulse is shown. (Right) ON gating currents recorded in the absence (■) or presence (○) of Mg^{2+} were integrated to obtain the gating charge (Q), which was normalized to the maximum charge obtained in the experiment, and plotted versus voltage. Data were fitted with the sum of two Boltzmann functions to obtain values for $V_{1/2}$ and apparent valence (z) for the q1 and q2 components of gating charge. Fitted parameters are provided in Table I.

the engineered binding site, has no significant impact on the major voltage-dependent conformational changes of the voltage sensor domain. This observation is consistent with the finding that residues critical for the surface charge effect of Mg^{2+} are located in and near the mouth of the Shaker pore (Elinder and Århem, 2003; Broomand et al., 2007).

Mg^{2+} affected the major voltage-dependent conformational changes of the voltage sensor domain only when bound within the plane of the membrane in proximity to the charge-moving arginine residues in S4 (Aggarwal and MacKinnon, 1996; Seoh et al., 1996). We found that Mg^{2+} significantly increased the apparent valence, z_1, of the q1 component of charge movement in I287D+F324D channels. In the absence of Mg^{2+}, z_1 for the double mutant was half that measured in W434F channels (Table I). One possible explanation for this result is that introducing negatively charged aspartate residues in S2 and S3b reduces the effective charge of nearby voltage-sensing arginine residues in S4 (Aggarwal and MacKinnon, 1996; Seoh et al., 1996). This would be consistent with the observation that Mg^{2+} binding restores z_1 in I287D+F324D channels to the value measured in W434F channels (Table I). The apparent valence, z_2, for the q2 component of charge movement was also reduced in I287D+F324D channels compared with the control, but this value was unchanged by Mg^{2+} binding.

Model of the Shaker divalent cation binding site

Because positions analogous to the binding site residues are closely apposed in the Kv1.2/Kv2.1 chimera x-ray structure, we used it as a scaffold to generate a threaded model of the Shaker voltage sensor domain (Fig. 10 A) (Eswar et al., 2006; Long et al., 2007). In this model, I287 and F324 are separated by ~4 Å at their closest point. To incorporate the ion binding site, I287 and F324 were mutated in silico to aspartate, a Mg^{2+} ion was manually positioned to achieve ideal bond distances of 2.2–2.4 Å, and the model was idealized using the program Refmac (Fig. 10, B and C) (Collaborative Computational Project, Number 4, 1994). In the binding site model, the closest side chain carboxylate oxygen atoms

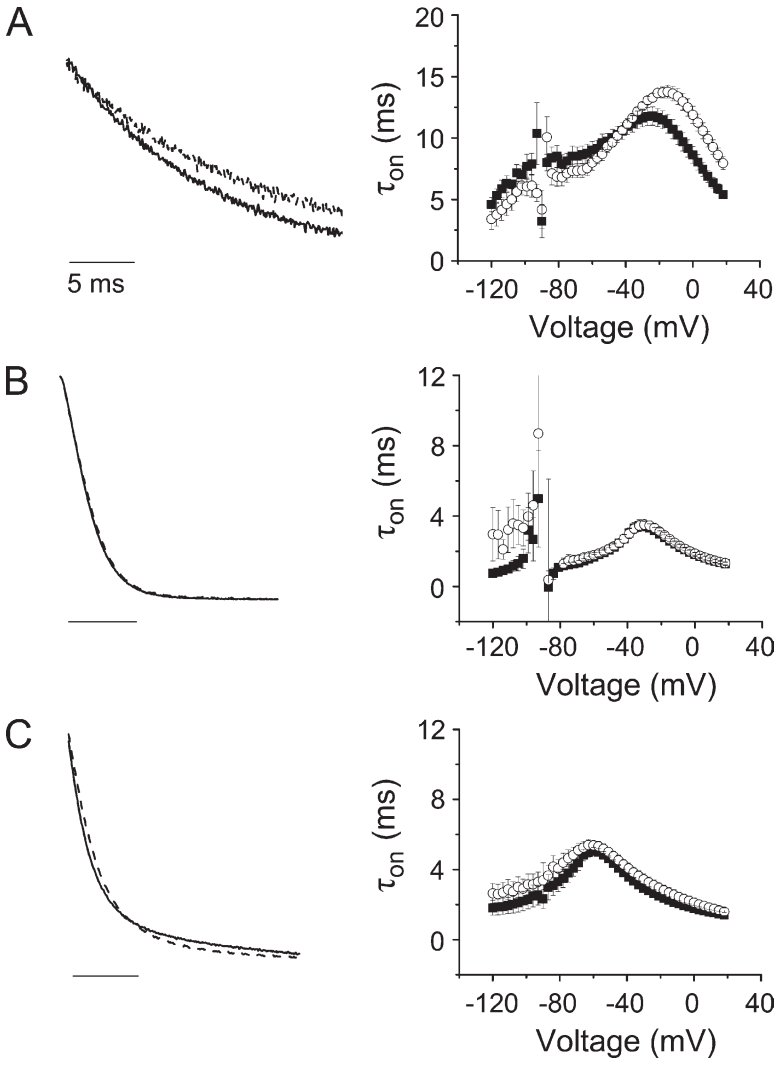

Figure 9. Mg^{2+} slows gating charge movement in I287D+F324D channels, but not in control (W434F) or I287D channels. Gating currents were recorded from (A) I287D+F324D, (B) W434F, or (C) I287D channels in the absence or presence of Mg^{2+} using the pulse protocols described in the Fig. 8 legend. (Left) Representative ON gating current traces obtained at −9 mV in the absence (solid trace) or presence (dashed trace) of Mg^{2+} have been scaled and overlaid. (Right) Gating current traces recorded in the absence (■) or presence (○) of Mg^{2+} were fitted with a single-exponential component to obtain values for τ_{on}, which have been plotted versus voltage. In A, values of τ_{on} measured in the presence and absence of Mg^{2+} differed significantly from −21 to +18 mV; $P < 0.05$ by ANOVA. Values of τ_{on} obtained at −9 mV are shown in Table II.

of I287D and F324D are ~3.8 Å apart. The average distance between Mg^{2+} and a carboxylate oxygen atom in the coordination sphere is ~2 Å, a value typically found in high resolution structures of Mg^{2+} binding sites (Dokmanić et al., 2008). Therefore, according to our threaded Shaker model, I287D and F324D are close enough to simultaneously coordinate a Mg^{2+} ion (Fig.10C). This model reflects the thermodynamically most stable conformation of the protein, presumably corresponding to an inactivated state, because the chimera was crystallized in the absence of a membrane potential (Long et al., 2007). When combined with our functional data indicating that Mg^{2+} binds to the resting state of the Shaker voltage sensor domain and modifies both phases of gating charge movement, the model confirms that the binding site residues remain in proximity throughout activation and inactivation.

One surprising aspect of the binding site model is that the aspartate residues, particularly F324D, are located at the interface between the voltage sensor domain and the hydrophobic core of the membrane. In commonly used hydrophobic indices, aspartate ranks as

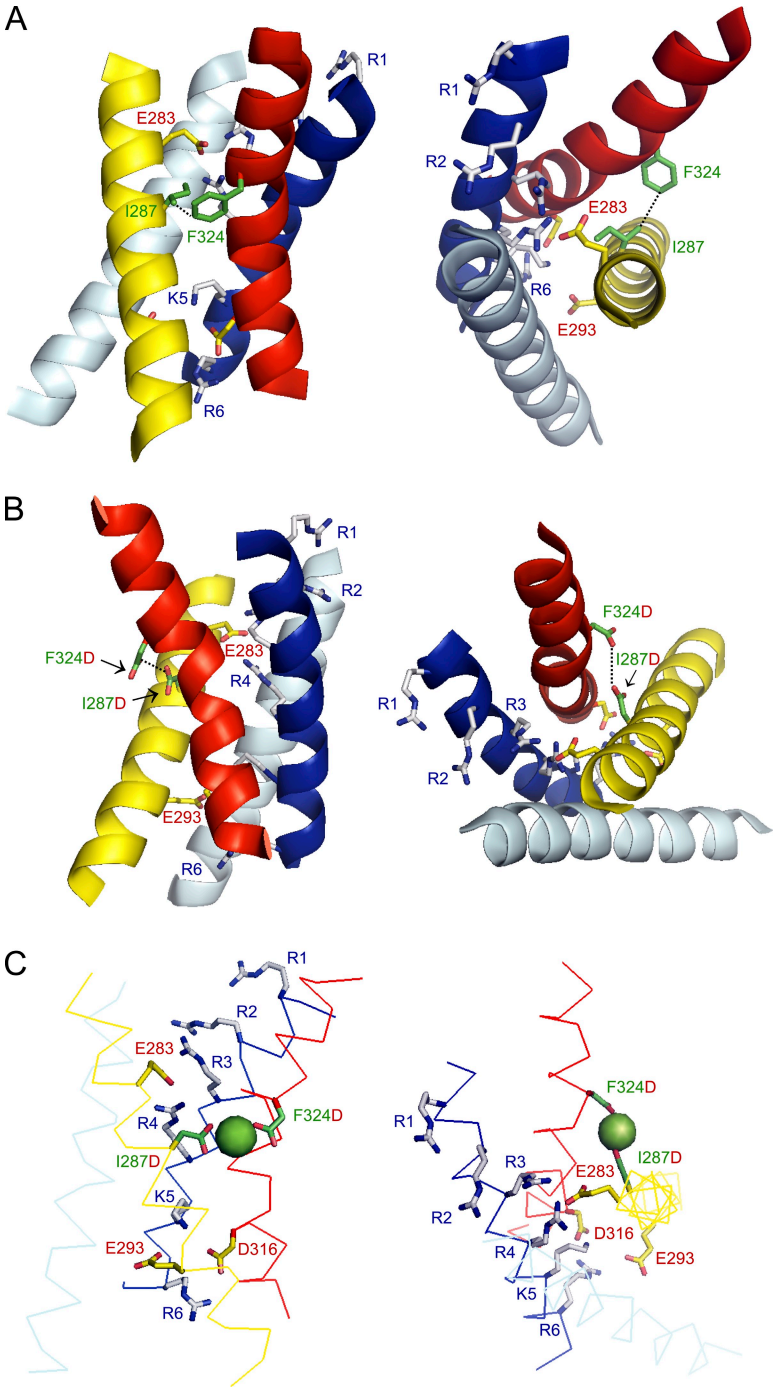

Figure 10. Threaded models of Shaker-IR and I287D+F324D based on Kv1.2/Kv2.1 chimera structure. (A) I287 and F324 are closely apposed in threaded Shaker-IR model. Side (left) and top (right) views are shown. S1 (light blue), S2 (yellow), S3 (red), and S4 (dark blue) transmembrane segments are pictured in cartoon form. Selected side chains are shown: I287 in S2 and F324 in S3b (green); acidic residues E283 and E293 in S2 and D316 in S3 (yellow and red); basic residues R362, R365, R368, R371, K374, and R377 in S4 (gray and blue). A subset of side chains are labeled to provide landmarks. S4 positively charged residues are labeled with a generic nomenclature (R1–R6). Dotted black line connects atoms of I287 and F324 that are ~4.0 Å apart. (B) Aspartate residues introduced at I287D and F324D are closely apposed and located at the interface between the voltage sensor domain and the hydrophobic core of the membrane. Side (left) and top (right) views of I287D+F324D double-mutant model. Color code and labeling are the same as in A, except that the mutations I287D and F324D are shown in green and red. Dotted black line connects oxygen atoms of D287 and D324 that are ~3.8 Å apart. (C) I287D and F324D are able to simultaneously coordinate a Mg^{2+} ion. Side (left) and top (right) views of I287D+F324D double-mutant model. Transmembrane segments S1–S4 are shown in ribbon form using the same color code as in A. Bound Mg^{2+} ion is shown as a green sphere. Color code and labeling are the same as in B. The figure was made using PyMOL (DeLano, 2002).

one of the most hydrophilic amino acids (Kyte and Doolittle, 1982; Engelman et al., 1986; Wimley and White, 1996). Indeed, in an experimentally determined scale, aspartate is the most difficult residue to insert into a membrane (Hessa et al., 2005). However, in eag, mutating either binding site aspartate to a neutral residue slows activation, mimicking ion binding (Silverman et al., 2000). This strongly suggests that the aspartate residues are ionized at physiological pH in the absence of a divalent cation. The same argument applies to the Shaker binding site. Charge shielding is fundamental to changing the time course of pore opening in Shaker because protonation of the binding site aspartate residues at pH 5.5 slows activation to the same extent as Mg^{2+} binding at pH 7.5 or 8.0. To reduce the energetic penalty incurred by ionized aspartate residues at the hydrophobic interface, S2 and/or S3b may twist away from the bilayer core in I287D+F324D. Upon ion binding, the relative orientation or flexibility of S2 and S3b may be altered. Molecular dynamics simulations of the model embedded in a lipid bilayer will be needed to investigate these issues.

Shaker binding site constrains closed-state structure and types of conformational changes that occur during activation

The proximity of I287 and F324 in different voltage sensor conformations provides an important criterion for evaluating models of the resting state and the conformational changes that occur during voltage-dependent activation in Shaker-type channels. Recently, several models for the closed state of Shaker channels have been proposed (Chanda et al., 2005; Yarov-Yarovoy et al., 2006; Campos et al., 2007; Pathak et al., 2007; Broomand and Elinder, 2008). We evaluated whether these models are compatible with the Shaker binding site constraint by mutating I287 and F324 in silico to aspartate and measuring the distances between carboxylate oxygens. Closed-state models proposed by Chanda et al. (2005) and Yarov-Yarovoy et al. (2006) are incompatible with our results. These models predict inter-oxygen distances of ~18 and ~13 Å, respectively. Not only is this too far for simultaneous coordination of Mg^{2+}, but other parts of the protein are interposed between positions 287 and 324 in these models. In contrast, the model proposed by Pathak et al. (2007) is more compatible with our results because the inter-oxygen distance is ~4–6 Å. However, on the basis of a voltage clamp fluorimetry scan, Pathak et al. (2007) propose a large movement of S3b relative to its environment during activation. Such a conformational change might be incompatible with our results, which indicate that positions 287 in S2 and 324 in S3b stay closely apposed throughout activation.

Our results do not support the paddle model for activation, in which S3b, assumed to start at P322 in Shaker (Fig. 1 A), is stably associated with S4 during activation (Jiang et al., 2003; Long et al., 2005b; Ruta et al., 2005; Alabi et al., 2007). Large movements of the paddle would likely separate F324 in S3b from I287 in S2, which does not agree with our findings.

Broomand and Elinder (2008) have reported that I325C forms state-dependent disulfide bonds with several cysteine mutations in S4. To accommodate their data, they propose that S3b in Shaker is rotated 60° in the counterclockwise direction compared with the Kv1.2/Kv2.1 chimera structure. This proposal is incompatible with our results because rotating S3b would separate the binding site residues and move an aspartate residue at position 324 from the protein–lipid interface to a position where the acidic side chain would project directly into the hydrophobic core of the membrane.

Interestingly, a cysteine introduced at binding site position 287 in S2 forms a disulfide bond with R362C, a mutation in the first charge-moving arginine residue in S4, in the resting state. Upon reduction of the disulfide bond, a low affinity Cd^{2+} binding site is formed (Campos et al., 2007). These data place R362 in the vicinity of the binding site in the resting conformation. This is compatible with the proposal that charge-moving S4 arginines sequentially inhabit a position near E283 in S2, one α-helical rung above binding site position 287, during voltage-dependent activation (Tiwari-Woodruff et al., 2000; Silverman et al., 2003; Tombola et al., 2005; Yarov-Yarovoy et al., 2006). Collectively, the available evidence strongly suggests that the first four arginines in S4, which carry the bulk of the gating charge in Shaker, move past the ion binding site during activation (Aggarwal and MacKinnon, 1996; Seoh et al., 1996). Thus, divalent cations are likely to affect S4 conformational changes directly, so that changes in the time course of activation are mediated locally rather than at a distance. The functional and mechanistic similarities between the engineered binding site in Shaker and naturally occurring binding site in eag indicate that the details of these conformational changes are well conserved among distantly related voltage-gated channels.

Coordinates

Coordinates for the threaded models of the Shaker-IR and I287D+F324D voltage sensor domains are available upon request.

We thank Drs. Benoit Roux and Vladimir Yarov-Yarovoy for sharing the coordinates of their closed-state models. We are grateful to Drs. Riccardo Olcese and Antonios Pantazis for their generous advice and assistance with gating current experiments, to Allan Mock for excellent technical assistance, and to members of the Papazian laboratory for comments on the manuscript.

This work was supported by National Institutes of Health grant R01 GM43459 (to D.M. Papazian).

Edward N. Pugh Jr. served as editor.

Submitted: 20 August 2009
Accepted: 29 March 2010

REFERENCES

Aggarwal, S.K., and R. MacKinnon. 1996. Contribution of the S4 segment to gating charge in the Shaker K^+ channel. *Neuron.* 16:1169–1177. doi:10.1016/S0896-6273(00)80143-9

Alabi, A.A., M.I. Bahamonde, H.J. Jung, J.I. Kim, and K.J. Swartz. 2007. Portability of paddle motif function and pharmacology in voltage sensors. *Nature.* 450:370–375. doi:10.1038/nature06266

Baker, O.S., H.P. Larsson, L.M. Mannuzzu, and E.Y. Isacoff. 1998. Three transmembrane conformations and sequence-dependent displacement of the S4 domain in shaker K^+ channel gating. *Neuron.* 20:1283–1294. doi:10.1016/S0896-6273(00)80507-3

Bannister, J.P.A., B. Chanda, F. Bezanilla, and D.M. Papazian. 2005. Optical detection of rate-determining ion-modulated conformational changes of the ether-à-go-go K^+ channel voltage sensor. *Proc. Natl. Acad. Sci. USA.* 102:18718–18723. doi:10.1073/pnas.0505766102

Bezanilla, F., and C.M. Armstrong. 1977. Inactivation of the sodium channel. I. Sodium current experiments. *J. Gen. Physiol.* 70:549–566. doi:10.1085/jgp.70.5.549

Bezanilla, F., E. Perozo, and E. Stefani. 1994. Gating of Shaker K^+ channels: II. The components of gating currents and a model of channel activation. *Biophys. J.* 66:1011–1021. doi:10.1016/S0006-3495(94)80882-3

Broomand, A., and F. Elinder. 2008. Large-scale movement within the voltage-sensor paddle of a potassium channel-support for a helical-screw motion. *Neuron.* 59:770–777. doi:10.1016/j.neuron.2008.07.008

Broomand, A., F. Österberg, T. Wardi, and F. Elinder. 2007. Electrostatic domino effect in the Shaker K channel turret. *Biophys. J.* 93:2307–2314. doi:10.1529/biophysj.107.104349

Campos, F.V., B. Chanda, B. Roux, and F. Bezanilla. 2007. Two atomic constraints unambiguously position the S4 segment relative to S1 and S2 segments in the closed state of Shaker K channel. *Proc. Natl. Acad. Sci. USA.* 104:7904–7909. doi:10.1073/pnas.0702638104

Chanda, B., O.K. Asamoah, R. Blunck, B. Roux, and F. Bezanilla. 2005. Gating charge displacement in voltage-gated ion channels involves limited transmembrane movement. *Nature.* 436:852–856. doi:10.1038/nature03888

Chandy, K.G., and G.A. Gutman. 1995. Voltage-gated potassium channel genes. *In* Ligand- and Voltage-Gated Ion Channels. R.A. North, editor. CRC Press, Boca Raton, FL. 1–71.

Collaborative Computational Project, Number 4. 1994. The *CCP4* suite: programs for protein crystallography. *Acta Crystallogr. D Biol. Crystallogr.* 50:760–763. doi:10.1107/S0907444994003112

DeLano, W.L. 2002. PyMOL Molecular Viewer. http://www.pymol.org (accessed March 30, 2010).

Dhallan, R.S., K.W. Yau, K.A. Schrader, and R.R. Reed. 1990. Primary structure and functional expression of a cyclic nucleotide-activated channel from olfactory neurons. *Nature.* 347:184–187. doi:10.1038/347184a0

Dokmanić, I., M. Sikić, and S. Tomić. 2008. Metals in proteins: correlation between the metal-ion type, coordination number and the amino-acid residues involved in the coordination. *Acta Crystallogr. D Biol. Crystallogr.* 64:257–263. doi:10.1107/S090744490706595X

Elinder, F., and P. Århem. 2003. Metal ion effects on ion channel gating. *Q. Rev. Biophys.* 36:373–427. doi:10.1017/S0033583504003932

Engelman, D.M., T.A. Steitz, and A. Goldman. 1986. Identifying nonpolar transbilayer helices in amino acid sequences of membrane proteins. *Annu. Rev. Biophys. Biophys. Chem.* 15:321–353. doi:10.1146/annurev.bb.15.060186.001541

Eswar, N., B. Webb, M.A. Marti-Renom, M.S. Madhusudhan, D. Eramian, M. Shen, U. Pieper, and A. Sali. 2006. Comparative protein structure modeling with MODELLER. *In* Current Protocols in Bioinformatics. John Wiley and Sons, Inc., New York. Supplement 15:5.6.1–5.6.30.

Hessa, T., H. Kim, K. Bihlmaier, C. Lundin, J. Boekel, H. Andersson, I. Nilsson, S.H. White, and G. von Heijne. 2005. Recognition of transmembrane helices by the endoplasmic reticulum translocon. *Nature.* 433:377–381. doi:10.1038/nature03216

Hoshi, T., W.N. Zagotta, and R.W. Aldrich. 1990. Biophysical and molecular mechanisms of Shaker potassium channel inactivation. *Science.* 250:533–538. doi:10.1126/science.2122519

Jiang, Y., V. Ruta, J. Chen, A. Lee, and R. MacKinnon. 2003. The principle of gating charge movement in a voltage-dependent K^+ channel. *Nature.* 423:42–48. doi:10.1038/nature01581

Kaupp, U.B., T. Niidome, T. Tanabe, S. Terada, W. Bönigk, W. Stühmer, N.J. Cook, K. Kangawa, H. Matsuo, T. Hirose, et al. 1989. Primary structure and functional expression from complementary DNA of the rod photoreceptor cyclic GMP-gated channel. *Nature.* 342:762–766. doi:10.1038/342762a0

Kyte, J., and R.F. Doolittle. 1982. A simple method for displaying the hydropathic character of a protein. *J. Mol. Biol.* 157:105–132. doi:10.1016/0022-2836(82)90515-0

Lainé, M., M.C. Lin, J.P.A. Bannister, W.R. Silverman, A.F. Mock, B. Roux, and D.M. Papazian. 2003. Atomic proximity between S4 segment and pore domain in Shaker potassium channels. *Neuron.* 39:467–481. doi:10.1016/S0896-6273(03)00468-9

Landt, O., H.P. Grunert, and U. Hahn. 1990. A general method for rapid site-directed mutagenesis using the polymerase chain reaction. *Gene.* 96:125–128. doi:10.1016/0378-1119(90)90351-Q

Lin, M.C., and D.M. Papazian. 2007. Differences between ion binding to eag and HERG voltage sensors contribute to differential regulation of activation and deactivation gating. *Channels (Austin).* 1:429–437.

Long, S.B., E.B. Campbell, and R. Mackinnon. 2005a. Crystal structure of a mammalian voltage-dependent Shaker family K^+ channel. *Science.* 309:897–903. doi:10.1126/science.1116269

Long, S.B., E.B. Campbell, and R. Mackinnon. 2005b. Voltage sensor of Kv1.2: structural basis of electromechanical coupling. *Science.* 309:903–908. doi:10.1126/science.1116270

Long, S.B., X. Tao, E.B. Campbell, and R. MacKinnon. 2007. Atomic structure of a voltage-dependent K^+ channel in a lipid membrane-like environment. *Nature.* 450:376–382. doi:10.1038/nature06265

Nelson, R.D., G. Kuan, M.H. Saier Jr., and M. Montal. 1999. Modular assembly of voltage-gated channel proteins: a sequence analysis and phylogenetic study. *J. Mol. Microbiol. Biotechnol.* 1:281–287.

Papazian, D.M., L.C. Timpe, Y.N. Jan, and L.Y. Jan. 1991. Alteration of voltage-dependence of Shaker potassium channel by mutations in the S4 sequence. *Nature.* 349:305–310. doi:10.1038/349305a0

Papazian, D.M., X.M. Shao, S.-A. Seoh, A.F. Mock, Y. Huang, and D.H. Wainstock. 1995. Electrostatic interactions of S4 voltage sensor in Shaker K^+ channel. *Neuron.* 14:1293–1301. doi:10.1016/0896-6273(95)90276-7

Pathak, M.M., V. Yarov-Yarovoy, G. Agarwal, B. Roux, P. Barth, S. Kohout, F. Tombola, and E.Y. Isacoff. 2007. Closing in on the resting state of the Shaker K^+ channel. *Neuron.* 56:124–140. doi:10.1016/j.neuron.2007.09.023

Perozo, E., R. MacKinnon, F. Bezanilla, and E. Stefani. 1993. Gating currents from a nonconducting mutant reveal open-closed conformations in Shaker K^+ channels. *Neuron.* 11:353–358. doi:10.1016/0896-6273(93)90190-3

Perozo, E., L. Santacruz-Toloza, E. Stefani, F. Bezanilla, and D.M. Papazian. 1994. S4 mutations alter gating currents of Shaker K channels. *Biophys. J.* 66:345–354. doi:10.1016/S0006-3495(94)80783-0

Ruta, V., J. Chen, and R. MacKinnon. 2005. Calibrated measurement of gating-charge arginine displacement in the KvAP voltage-dependent K^+ channel. *Cell.* 123:463–475. doi:10.1016/j.cell.2005.08.041

Seoh, S.A., D. Sigg, D.M. Papazian, and F. Bezanilla. 1996. Voltage-sensing residues in the S2 and S4 segments of the Shaker K^+ channel. *Neuron.* 16:1159–1167. doi:10.1016/S0896-6273(00)80142-7

Silverman, W.R., C.-Y. Tang, A.F. Mock, K.-B. Huh, and D.M. Papazian. 2000. Mg^{2+} modulates voltage-dependent activation in ether-à-go-go potassium channels by binding between transmembrane segments S2 and S3. *J. Gen. Physiol.* 116:663–678. doi:10.1085/jgp.116.5.663

Silverman, W.R., B. Roux, and D.M. Papazian. 2003. Structural basis of two-stage voltage-dependent activation in K^+ channels. *Proc. Natl. Acad. Sci. USA.* 100:2935–2940. doi:10.1073/pnas.0636603100

Silverman, W.R., J.P.A. Bannister, and D.M. Papazian. 2004. Binding site in eag voltage sensor accommodates a variety of ions and is accessible in closed channel. *Biophys. J.* 87:3110–3121. doi:10.1529/biophysj.104.044602

Stefani, E., L. Toro, E. Perozo, and F. Bezanilla. 1994. Gating of Shaker K^+ channels: I. Ionic and gating currents. *Biophys. J.* 66:996–1010. doi:10.1016/S0006-3495(94)80881-1

Tang, C.-Y., F. Bezanilla, and D.M. Papazian. 2000. Extracellular Mg^{2+} modulates slow gating transitions and the opening of *Drosophila* ether-à-go-go potassium channels. *J. Gen. Physiol.* 115:319–338. doi:10.1085/jgp.115.3.319

Tempel, B.L., D.M. Papazian, T.L. Schwarz, Y.N. Jan, and L.Y. Jan. 1987. Sequence of a probable potassium channel component encoded at the *Shaker* locus of *Drosophila*. *Science.* 237:770–775. doi:10.1126/science.2441471

Terlau, H., J. Ludwig, R. Steffan, O. Pongs, W. Stühmer, and S.H. Heinemann. 1996. Extracellular Mg^{2+} regulates activation of rat eag potassium channel. *Pflugers Arch.* 432:301–312. doi:10.1007/s004240050137

Timpe, L.C., T.L. Schwarz, B.L. Tempel, D.M. Papazian, Y.N. Jan, and L.Y. Jan. 1988. Expression of functional potassium channels from *Shaker* cDNA in *Xenopus* oocytes. *Nature.* 331:143–145. doi:10.1038/331143a0

Tiwari-Woodruff, S.K., C.T. Schulteis, A.F. Mock, and D.M. Papazian. 1997. Electrostatic interactions between transmembrane segments mediate folding of Shaker K^+ channel subunits. *Biophys. J.* 72:1489–1500. doi:10.1016/S0006-3495(97)78797-6

Tiwari-Woodruff, S.K., M.A. Lin, C.T. Schulteis, and D.M. Papazian. 2000. Voltage-dependent structural interactions in the Shaker K^+ channel. *J. Gen. Physiol.* 115:123–138. doi:10.1085/jgp.115.2.123

Tombola, F., M.M. Pathak, and E.Y. Isacoff. 2005. Voltage-sensing arginines in a potassium channel permeate and occlude cation-selective pores. *Neuron.* 45:379–388. doi:10.1016/j.neuron.2004.12.047

Warmke, J.W., and B. Ganetzky. 1994. A family of potassium channel genes related to eag in Drosophila and mammals. *Proc. Natl. Acad. Sci. USA.* 91:3438–3442. doi:10.1073/pnas.91.8.3438

Warmke, J., R. Drysdale, and B. Ganetzky. 1991. A distinct potassium channel polypeptide encoded by the Drosophila eag locus. *Science.* 252:1560–1562. doi:10.1126/science.1840699

Wimley, W.C., and S.H. White. 1996. Experimentally determined hydrophobicity scale for proteins at membrane interfaces. *Nat. Struct. Biol.* 3:842–848. doi:10.1038/nsb1096-842

Yarov-Yarovoy, V., D. Baker, and W.A. Catterall. 2006. Voltage sensor conformations in the open and closed states in ROSETTA structural models of $K(^+)$ channels. *Proc. Natl. Acad. Sci. USA.* 103:7292–7297. doi:10.1073/pnas.0602350103